NOAA Technical Memorandum NESS 86

A SCHEME FOR ESTIMATING CONVECTIVE RAINFALL
FROM SATELLITE IMAGERY

Washington, D.C.
April 1977

noaa NATIONAL OCEANIC AND
ATMOSPHERIC ADMINISTRATION / National Environmental
Satellite Service

NESS 63 Snow Depth and Sno... ... David F. McGinnis, Jr., John A. Pritchard, ...y 1975, ...M-75-10482/AS)

NESS 64 Central Processin... ...Satellit... ...harles F. Bristor (Editor), March 1975, 155 ...

NESS 65 Geographical Rel... ...d a Point View...pendicular to the Satellite Velocity Vector (... ...d Gruber, Mar...5, 14 pp. (COM-75-10678/AS) 10678/AS)

NESS 66 A Summary of the ... ...l of the C...ce in the Microwave Region. John C. Alishouse, ...10849/AS)

NESS 67 Data Collection Sy... ...l ... ...llite: Preliminary Report. Merle L. Nelson, M... ...

NESS 68 Atlantic Tropical ... ...is for 1974. Donald ... Donald R. Cochran, James B. Lushine, Samue... ...ur C. Pike, and Kenneth O. ... April 1975, 6 pp. (COM-75-1-676/AS)

NESS 69 Publications and Final Reports on Contracts and Grants, NESS-1974. April 1975, 7 pp. (COM-75-10850/AS)

NESS 70 Dependence of VTPR Transmittance Profiles and Observed Radiances on Spectral Line Shape Parameters. Charles Braun, July 1975, 17 pp.

NESS 71 Nimbus-5 Sounder Data Processing System, Part II: Results. W. L. Smith, H. M. Woolf, C. M. Hayden, and W. C. Shen. July 1975, 102 pp.

NESS 72 Radiation Budget Data From the Meteorological Satellites, ITOS 1 and NOAA 1. Donald H. Flanders and William L. Smith, August 1975, 22 pp.

NESS 73 Operational Processing of Solar Proton Monitor Data. Stanley R. Brown, September 1975. (Revision of NOAA TM NESS 49), 15 pp.

NESS 74 Monthly Winter Snowline Variation in the Northern Hemisphere from Satellite Records, 1966-75. Donald R. Wiesnet and Michael Matson, November 1975, 21 pp. (PB-248437)

NESS 75 Atlantic Tropical and Subtropical Cyclone Classifications for 1975. D. C. Gaby, J. B. Lushine, B. M. Mayfield, S. C. Pearce, and K. O. Poteat, March, 1976, 14 pp.

NESS 76 The Use of the Radiosonde in Deriving Temperature Soundings From the Nimbus and NOAA Satellite Data. Christopher M. Hayden, April 1976, 21 pp. (PB-256755)

NESS 77 Algorithm for Correcting the VHRR Imagery for Geometric Distortions Due to the Earth's Curvature and Rotation. Richard Legeckis and John Pritchard, April 1976, 30 pp.

NESS 78 Satellite Derived Sea-Surface Temperatures From NOAA Spacecraft. Robert L. Brower, Hilda S. Gohrband, William G. Pichel, T. L. Signore, and Charles C. Walton, in press, 1975.

NESS 79 Publications and Final Reports on Contracts and Grants, 1975. NESS, June 1976.

NESS 80 Satellite Images of Lake Erie Ice: January-March 1975. Michael C. McMillan and David Forsyth, June 1976.

NESS 81 Estimation of Daily Precipitation Over China and the USSR Using Satellite Imagery.   Walton A. Follansbee, September 1976, 37 pp.   (PB-261970/AS)

NESS 82 The GOES Data Collection System Platform Address Code. Wilfred E. Mazur, Jr., October 1976, 26 pp.   (PB-261968/AS)

NESS 83 River Basin Snow Mapping at the National Environmental Satellite Service. Stanley R. Schneider, Donald R. Wiesnet, and Michael C. McMillan, November, 1976, 27 pp. (PB-263816)

NESS 84 Winter Snow-Cover Maps of North America and Eurasia From Satellite Records, 1966-1976. Michael Matson, March 1977.

NESS 85 A Relationship Between Weakening of Tropical Cyclone Cloud Patterns and Lessening of Wind Speed. James B. Lushine, March 1977, 12 pp.
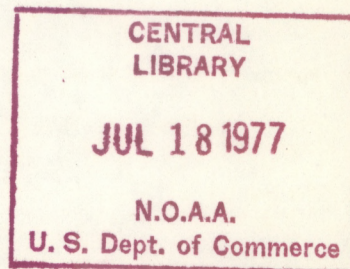
NOAA Technical Memorandum NESS 86

A SCHEME FOR ESTIMATING CONVECTIVE RAINFALL
FROM SATELLITE IMAGERY

Roderick A. Scofield
Vincent J. Oliver
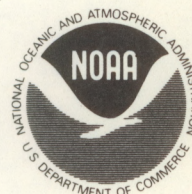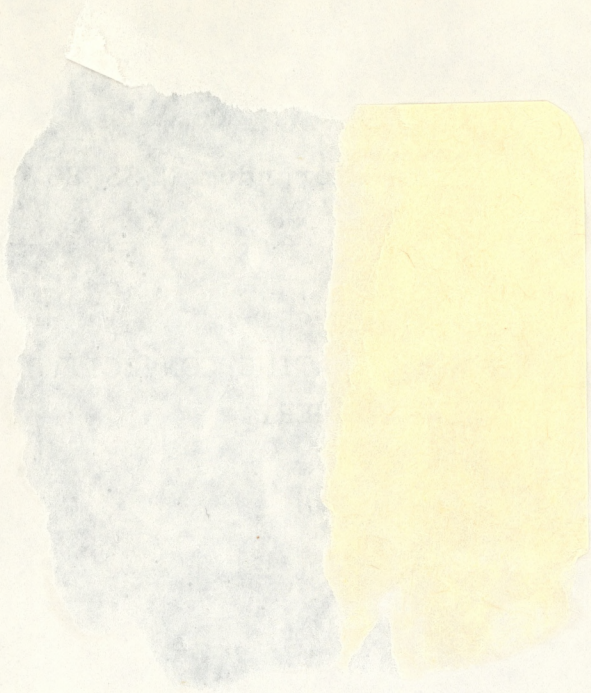
Applications Group
Washington, D.C.
April 1977

CONTENTS

A SCHEME FOR ESTIMATING CONVECTIVE RAINFALL
FROM SATELLITE IMAGERY

Roderick A. Scofield and Vincent J. Oliver
Applications Group, National Environmental Satellite Service,
National Oceanic and Atmospheric Administration
Washington, D.C.

ABSTRACT. During the past two years, the improvements
in processing satellite infrared (IR) data from syn-
chronous weather satellites have made possible a quan-
titative evaluation of cloud heights. Using these new
data and prior research on estimating rainfall from
visible satellite data, we have developed a simple,
quick method for obtaining rainfall estimates from
enhanced IR satellite images.

Starting with the simple empirical relationship that
the higher the top of the cloud (cumulonimbus) the
heavier the rain, we have added factors which greatly
improve the initial relationship. The two most impor-
tant factors are rate of anvil growth and position of
the cumulonimbus under the spreading anvil. Adding to
these the importance of merging cells, merging convec-
tive cloud lines, and overshooting tops, we have the
information needed to describe where and how much rain
has fallen. These factors are put together in the
form of a flow diagram (decision tree) which leads the
user to the box containing the appropriate answer for
a particular point.

I.   INTRODUCTION

The objective of this investigation is to develop a scheme for estimating
local convective rainfall from synchronous meteorological satellite imagery.

These satellite-derived rainfall estimates may supplement other data or
even, in some important cases, may be the only data available. The esti-
mation of rainfall is a primary concern in agricultural areas around the
world. Also, of utmost importance is the need to locate areas of heavy rain-
fall for making estimates for the issuance of flash flood warnings and to
evaluate or predict flood potential.

Various types of data are available for estimating the areal accumulation
of rainfall. These include rain gauge measurements, and radar and satellite
images. However, because of the spotty distribution of heavy showers, rain-
fall observations from relatively isolated rain gauges are not representative
of the true areal accumulation. Radar provides data of high resolution in
both space and time but is limited in areal coverage and is unreliable during

meteorological conditions that produce anomalous propagation. Satellites provide continuous observations of the clouds but not of the rain in time and space at the right resolution. Precipitating clouds must be inferred from cloud types and the way they change with time. This report describes an operational method for doing this.

Several investigators, commencing their work in the late 1960s, showed that estimating rainfall from both geosynchronous and polar-orbiting satellites was feasible. Estimates for convective rainfall are best derived from the half-hourly pictures available from the geosynchronous satellites. Less detailed estimates can be derived using once or twice per day pictures from polar-orbiting satellites. To make estimates for short time intervals, it is necessary to be able to separate precipitating from non-precipitating clouds and to pinpoint areas where instantaneous precipitation is heaviest. The emphasis in the late 1960s to the present has been on the development of a scheme to pinpoint rain areas.

A complete review of rainfall schemes which use either visible or IR satellite imagery is presented by Martin and Scherer (1973). Since then, additional progress has been accomplished by Martin et al. (1975), Follansbee and Oliver (1975), Oliver and Scofield (1976), Griffith et al. (1976), and Follansbee (1976). Most of the following important facts about rain clouds have been extracted from Woodley et al. (1972) for use in the present estimation scheme.

(1) Bright clouds in the visible imagery produce more rainfall than darker clouds.

(2) Bright clouds in the visible and clouds with cold tops in the IR imagery which are expanding in areal coverage (in early and mature stages of development) produce more rainfall than those not expanding.

(3) Decaying clouds produce little or no rainfall.

(4) Clouds with cold tops in the IR imagery produce more rainfall than those with warmer tops.

(5) Clouds with cold tops that are becoming warmer produce little or no rainfall.

(6) Merging of cumulonimbus (Cb) clouds increases the rainfall rate of the merging clouds.

(7) Most of the significant rainfall occurs in the upwind (at anvil level) portion of a convective system. The highest and coldest clouds form where the thunderstorms are most vigorous and the rain heaviest. These cold clouds get thinner downwind and look warmer in IR imagery as the anvil material blows away from its origin over the updraft.

This study of quantitative precipitation estimation uses much of the research done previously in conjunction with newly available enhanced IR imagery. The Applications Group of NESS has developed several enhanced IR

displays which make thunderstorm top temperatures more quantitatively deter-
minable from IR images. The enhancement used for this study contours the
cold convective cloud tops to show their temperatures (or heights). The warm
portion of the imagery is displayed using a nearly linear relationship be-
tween temperature and picture brightness (dark for warm and white for cold)
up to the edge temperature of Cb anvils (about -30°C). Above this temperature,
contours using various shades of gray show the temperature of the anvil.

Two enhancement curves with examples of their effect are presented in
figures 1-a through 1-f. The analog enhancement curve used during the summer
of 1975 is shown in figure 1-a; the digital enhancement curve, called Mb, is
displayed in figure 1-b. The Mb curve is used to produce the IR enhancement
employed in the convective rainfall estimation scheme described herein. Com-
parison of the enhanced and regular IR pictures shows that the coldest por-
tions and the temperature gradients in the Cb anvil are readily detectable in
the enhanced views; the ability to rapidly and accurately interpret satellite
imagery is very important in an operational environment. The convective rain-
fall estimate system was developed using such enhanced IR pictures. High
resolution visible imagery was used to refine the rainfall estimate obtained
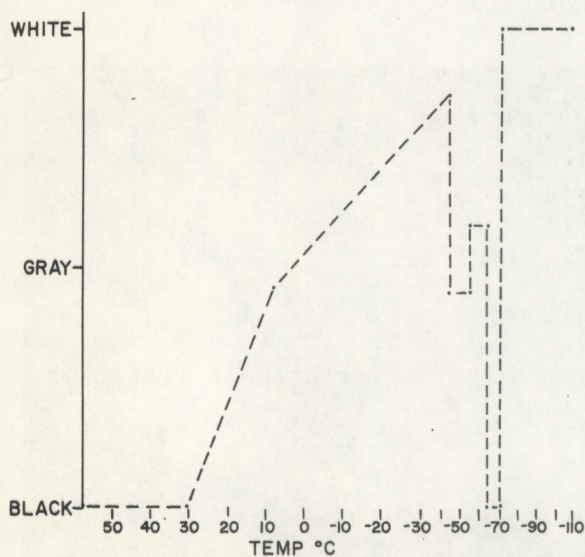from the IR pictures.

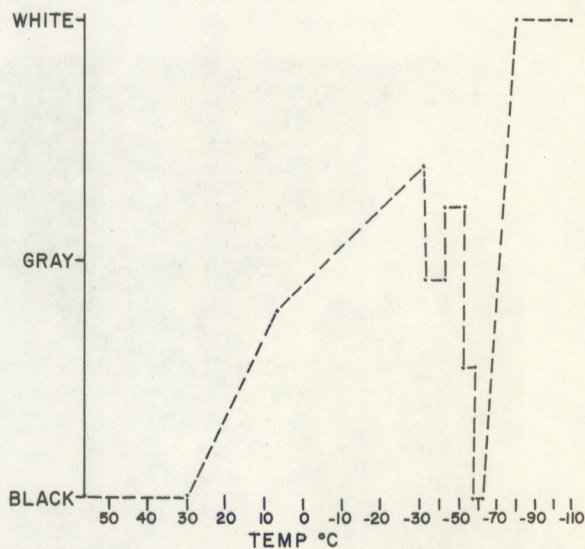Figure 1a.--Analog Enhancement Curve
(Summer 1975).

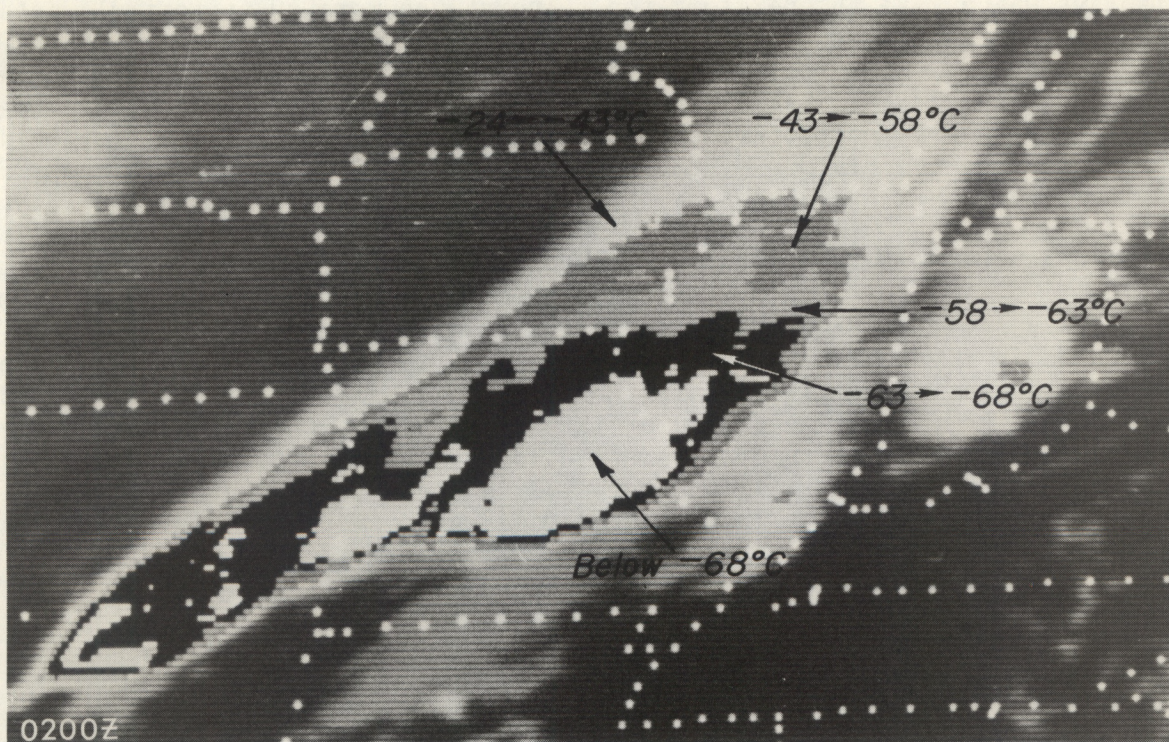Figure 1b.--Digital Enhancement
Curve (Mb).

Figure 1c.--Enlarged area from full disk IR image displayed using analog enhancement, 0200 GMT, 26 August 1975.
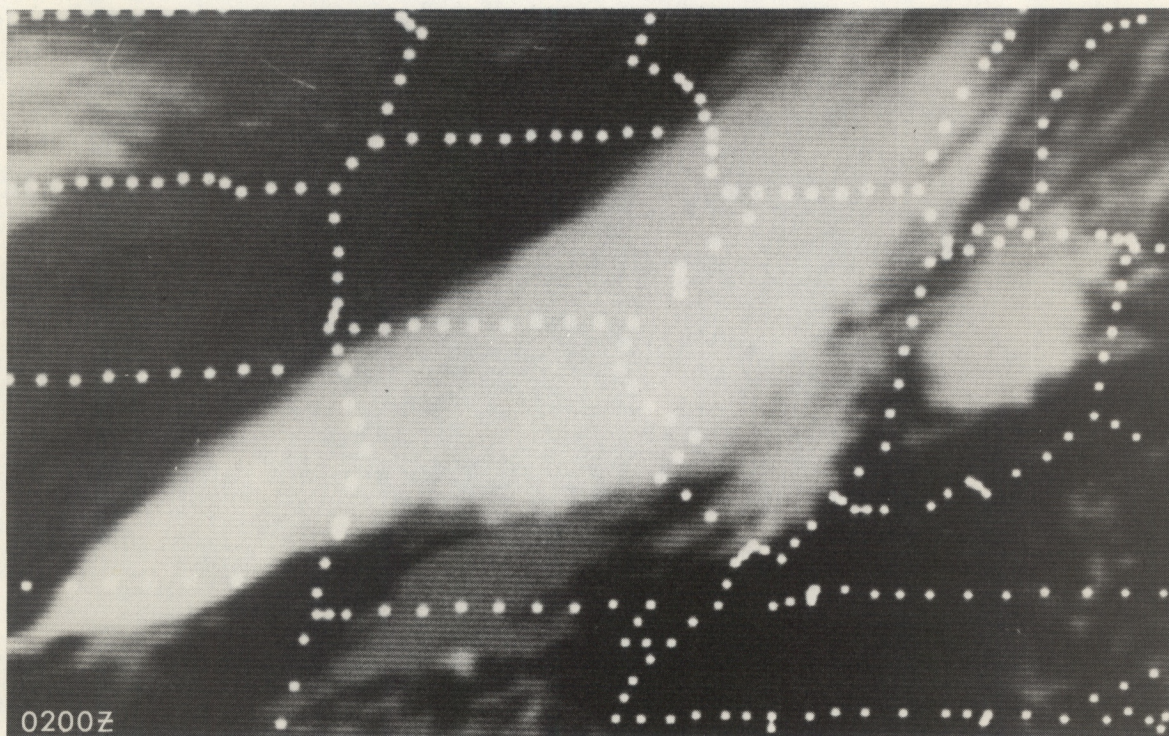

Figure 1d.--Enlarged area from full disk regular IR image, 0200 GMT, 26 August 1975.
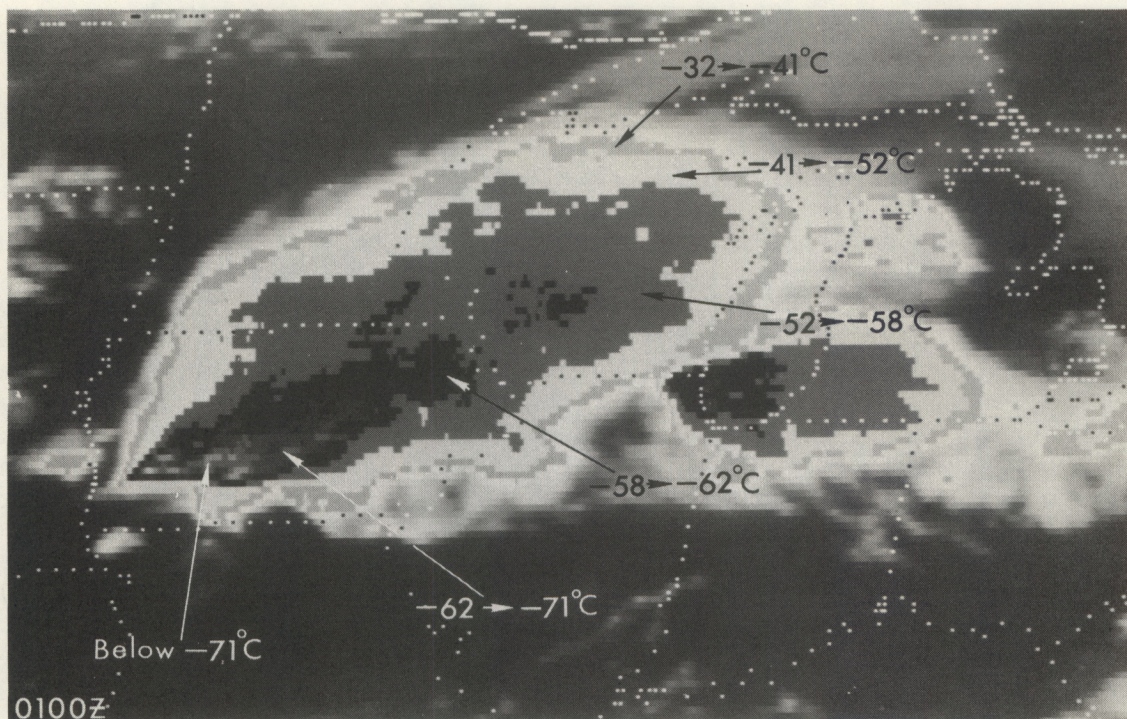
4

Figure 1e.--Enlarged area from 2-km equivalent IR produced using digital enhancement (Mb curve), 0100 GMT, 14 June 1976.
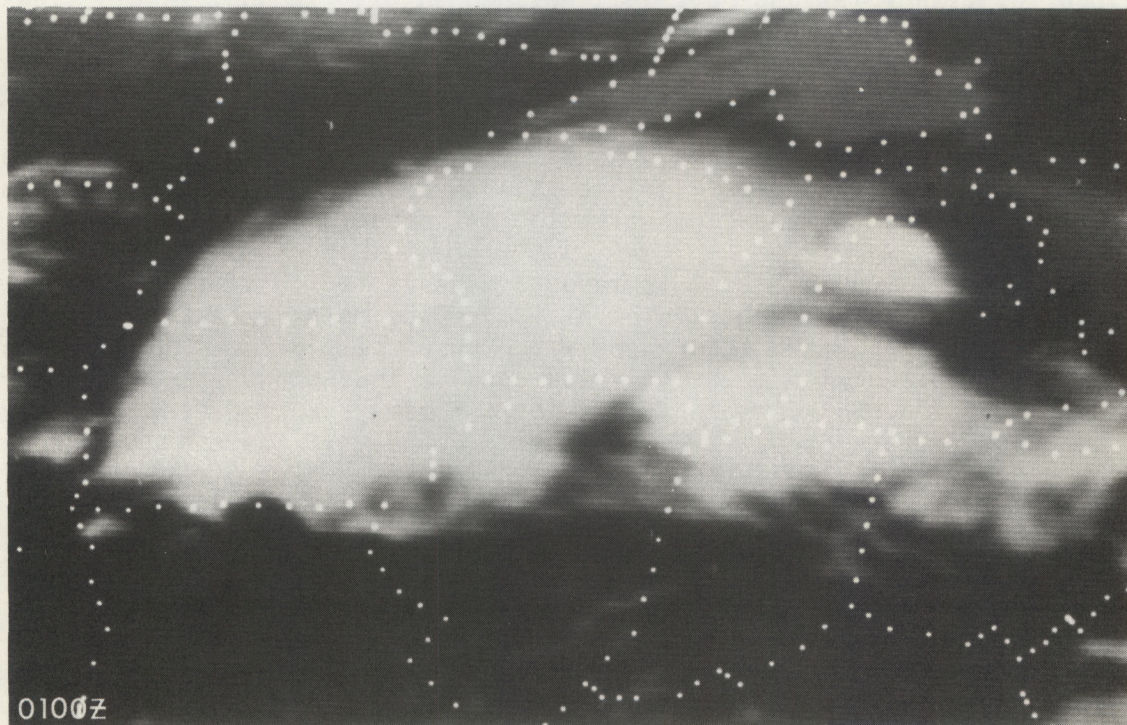

Figure 1f.--Enlarged area from full disk, regular IR image, 0100 GMT, 14 June 1976.

5

II. A QUANTIFIED PRECIPITATION ESTIMATION (QPE) SCHEME USING ENHANCED IR AND HIGH RESOLUTION VISIBLE IMAGERY

The method developed is for estimating half-hourly convective rainfall amounts (in inches) at a station (or point) by analyzing the ongoing changes in two consecutive (half-hourly) satellite pictures. We present it in the form of a flow diagram or decision tree in an appendix. Most of the data used to develop and test the methods came from the central part of the United States during the months of June through September. The rainfall estimates in the decision tree represent initial values (in inches) from one season's data and are based on the averages of from 20 to 40 samples, physical reasoning, and limited testing that helped to zero in on better estimate values.

The scheme is affected by cloud base level, the height of the tropopause, and orographic effects. For example, Cb clouds with cold tops over Minnesota may produce less rainfall than Cbs with the same top temperatures over the Gulf States where the cloud base is much lower. Also, clouds with cold tops over areas where uplift is due to orographic effects may produce extreme rainfall not accounted for in this scheme. Finally, the scheme was designed for summer tropopauses between -60 to -66°C.

Figure 2: Steps 1 and 2 of the Decision Tree.

The first decision in Step 1 is to determine from the half-hourly enhanced IR and visible imagery whether the cloud over the station is convective. In satellite pictures, convective clouds are quite often round, oval, carrot-shaped, or triangular and have well-defined edges. IR and visible views of the various stages of convective cloud clusters (C) are shown in figures 3-a through 3-f (other convective clouds in this sequence have not been singled out). Notice how the size, IR temperature contours and brightness in the visible imagery of each thunderstorm cluster changes with time. Also, at 2200 GMT some portions of the Cb anvils in the visible imagery (figure 3-f) appear to be more textured (e.g., at (T)) as compared to the remainder of the anvil. If the cloud under investigation is convective, proceed to Step 2.

The next decision in Step 2 is to determine if the convection over the station during the half-hour interval is deep by using enhanced IR. If the cloud top does not reach the range of contoured temperatures (colder than -32°C), convection with relatively low tops is indicated. A half-hourly rainfall amount of 0.05 inches (enter in Total Estimate Box of Step 6 on page 32) is assigned to this convective, unenhanced cloud. If the cloud top does reach the contoured range (colder than -32°C), proceed to Step 3.

Figure 4: Step 3 of the Decision Tree.

The next decision is to determine if the station is under the active, upwind portion of the convective cloud system by using enhanced IR and visible imagery. This step is the most subjective portion of the decision tree and takes some experience before one has complete confidence and can rapidly determine that a station is under the active or inactive portion of the Cb system.

The active portion of a convective system is the area of strong updrafts
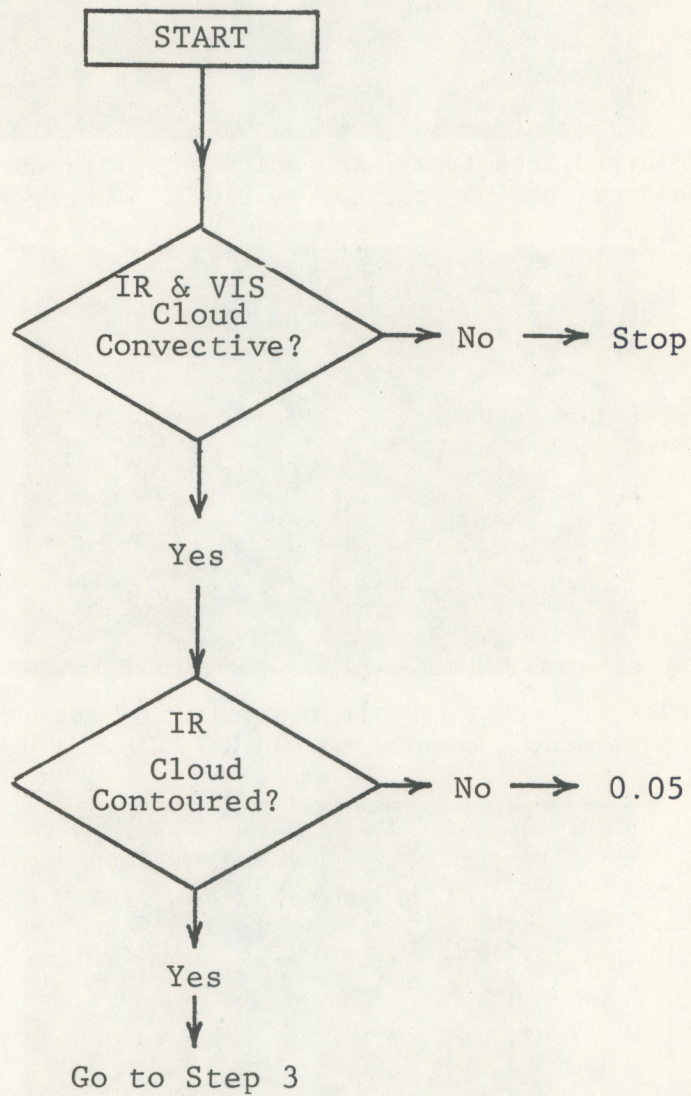
DECISION TREE

STEPS 1 and 2

```
┌─────────────┐
│    START    │
└─────────────┘
       │
       ▼

   ◇ IR & VIS
     Cloud          ──▶  No  ──▶  Stop
   Convective? ◇
       │
       ▼
      Yes
       │
       ▼

     ◇  IR
       Cloud        ──▶  No  ──▶  0.05
     Contoured? ◇
       │
       ▼
      Yes
       │
       ▼
   Go to Step 3
```
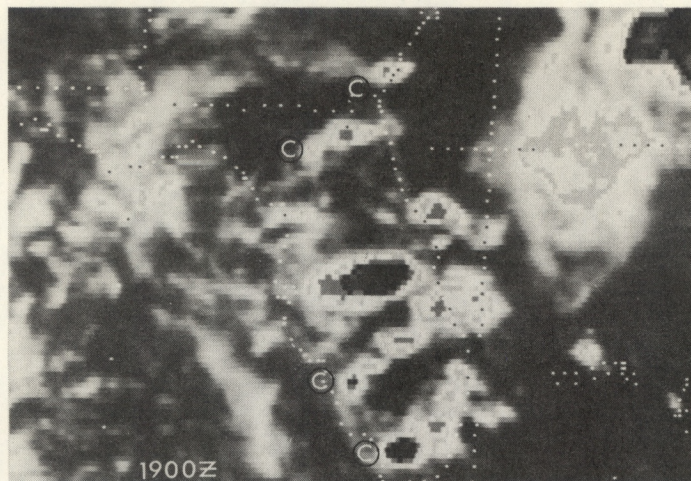
Figure 2.--Steps 1 and 2 of the Decision Tree.

7

Figure 3a.--Enlarged area from 2-km equivalent IR produced using digital enhancement (Mb curve), 1900 GMT, 19 July 1976.
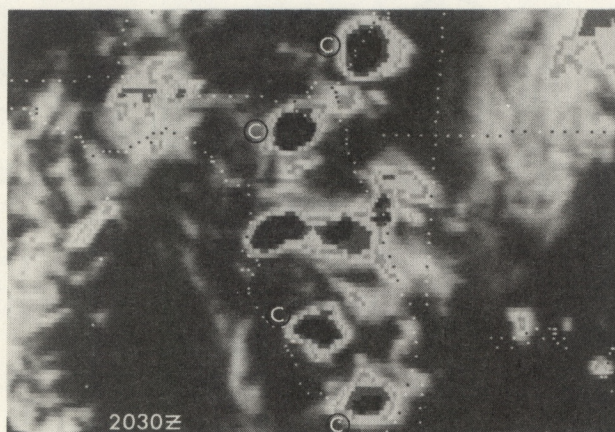

Figure 3b.--Enlarged area from 2-km equivalent IR produced using digital enhancement (Mb curve), 2030 GMT, 19 July 1976.
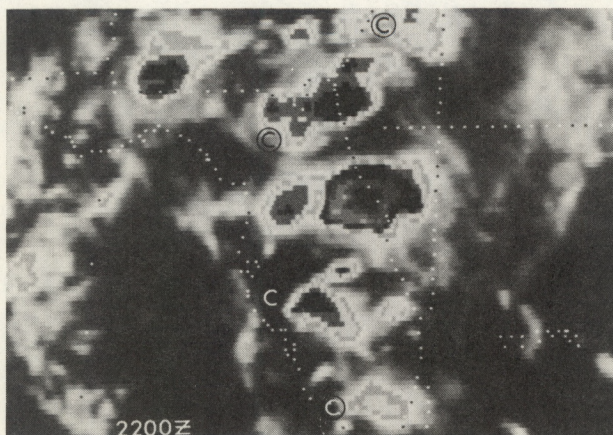

Figure 3c.--Enlarged area from 2-km equivalent IR produced using digital enhancement (Mb curve), 2200 GMT, 19 July 1976.
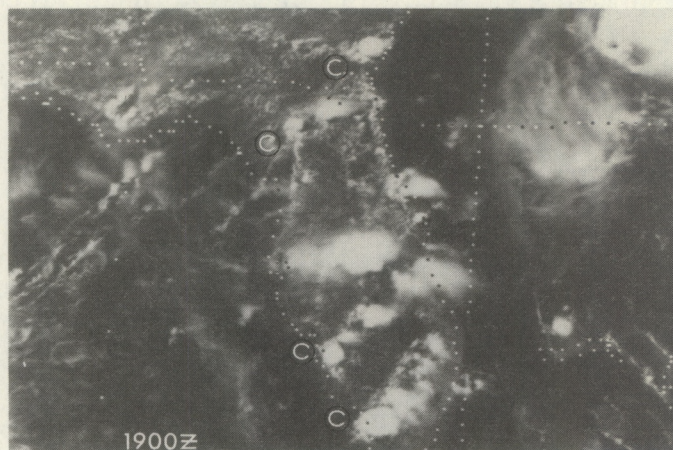
8

Figure 3d.--Enlarged area from 2-km visible imagery, 1900 GMT, 19 July 1976.
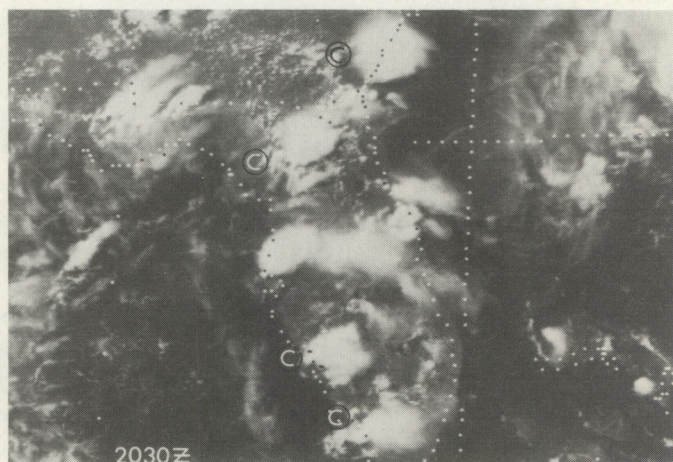

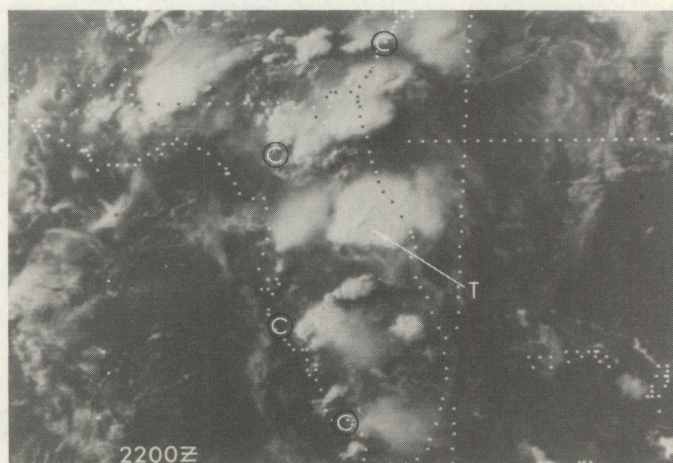Figure 3e.--Enlarged area from 2-km visible imagery, 2030 GMT, 19 July 1976.

Figure 3f.--Enlarged area from 2-km visible imagery, 2200 GMT, 19 July 1976.

and coincides with the heavy rain portion of the Cb under the spreading anvil and most often falls along the upwind edge of the anvil. The wind referred to here is the shear wind between the motion of the thunderstorm and the anvil level wind. The anvil stretches or elongates along the shear wind direction.

The upwind portion of the anvil is the place where the rain is most likely to be significant; little or no rain occurs in the downwind portion. The picture in figure 5 shows a Cb system photographed by Fujita near Salina, Kansas, 1915 CST, 5 May 1965. In figure 5, the significant rainfall is associated with the highest (coldest) tops in the upwind portion at (A); little or no rainfall occurs under the anvil area (B) tapering off downwind. An IR satellite picture of the Cb system in figure 5 would show a tight temperature gradient between the coldest (highest) tops at (A) and the cloud edge of the Cb; the temperature gradient in the direction of the anvil spreading downwind at (B) would be much less. The Cb system in figure 5 at (A) is quite thick and has turrets protruding above the anvil; the anvil gets thinner and its tops smoother in the downwind direction at (B). A visible satellite picture of this Cb system would show (A) to be bright and/or textured with overshooting tops; downwind at (B) would be darker and smoother.

Clues for helping us determine if the station is under the active portion of the convective system are listed below.

Clue 1: IR temperature gradient is tightest around station end of anvil (IR).

The upwind portion appears in the enhanced IR as the area of coldest temperature and is bounded by a tight temperature gradient. The downwind portion represents the anvil area which spreads out downstream from the active Cb cores. This downwind portion appears in the enhanced IR as an area of warmer temperatures and weaker temperature gradient.

In an incipient Cb, the cloud top is so small that upwind and downwind areas cannot be differentiated. When the storm is over 30 minutes old, the downwind area can become much larger than the upwind portion. When a thunderstorm system persists for a long time, the downwind area can become so large that the upwind area becomes less than one-tenth the size of the downwind area. The size of the upwind and downwind portions are controlled by the intensity of the system and the strength of the vertical wind shear.

In figures 6-a, 7-a and 8-a, the upwind portion of convective systems is shown by letters (A) and the downwind portion by letters (B). Radar data in figures 6-b, 7-b and 8-b show the significant rain areas (heaviest rain contours) in the upwind portion and areas of little or no rain in the downwind portion. Note the upwind portion of the convective system is bounded by a tight IR temperature gradient and the downwind portion by a weaker gradient.

For the case of little or no vertical wind shear, the IR temperature gradient is fairly uniform around the storm system and the heaviest rainfall is near the middle of the anvil where the tops are highest (coldest). The thunderstorm system in figure 9-a has its coldest tops near the center (A) of the Cb system. Also, note that the IR temperature gradient between the colder

STEP 3

```
┌─────────────────────────────┐
│  Locate active portion using │
│     the following clues      │
└─────────────────────────────┘
```

```
┌─────────────────────────────┐
│                             │
│  1.  Tight IR gradient (IR). │
│                             │
│  2.  Overshooting tops (VIS │
│      and IR).               │
│                             │
│  3.  Bright and/or more     │
│      textured (VIS).        │
│                             │
│  4.  Edge which moves least  │
│      (IR).                  │
│                             │
│  5.  300 mb upwind end (IR). │
│                             │
└─────────────────────────────┘
```

```
        Is station
        under active  ──No──► 0.01
         portion?

           Yes
```

```
┌─────────────────────────────┐
│        GO TO STEP 4          │
└─────────────────────────────┘
```
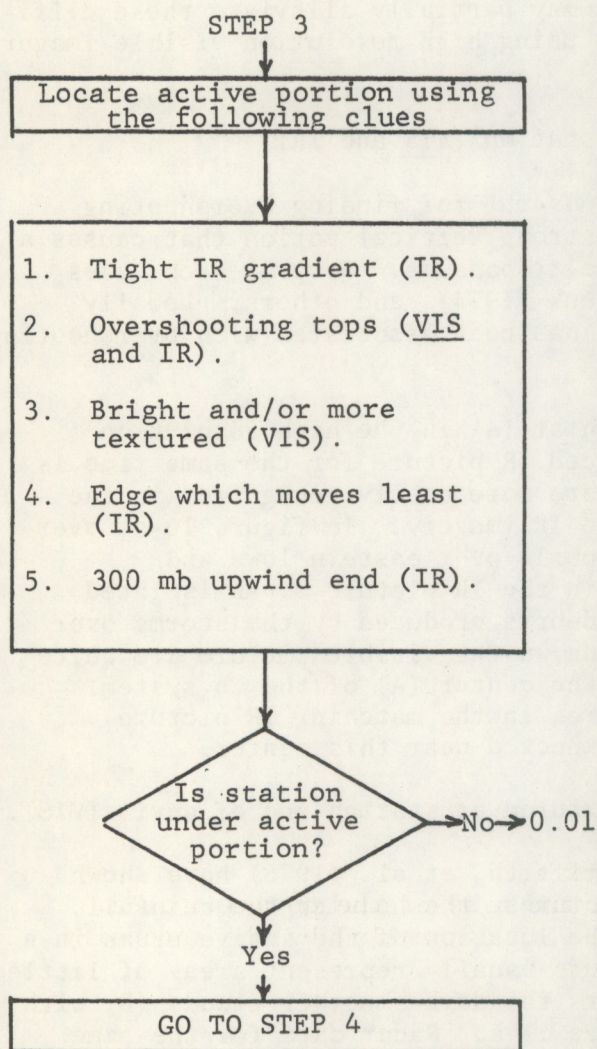
Figure 4.--Step 3 of the
Decision Tree

Figure 5.--Cumulonimbus cluster with overshooting tops and anvil debris, taken near Salina, Kansas, 1915 CST, 5 May 1965 (courtesy of Dr. T. Fujita).

11

and warmer contours of this Cb system is fairly uniform. High resolution visible imagery showing the same Cb system 30 minutes earlier is presented in figure 9-b.

There are situations when the upwind portion of the convective system is difficult to find because: (1) the maximum temperature gradients cannot be discerned or (2) the coldest contoured tops in the IR imagery overspread a large area. These situations are frequently encountered where numerous anvils spread into each other. Additional clues may partially alleviate these difficulties by animating the IR imagery or by using high resolution visible imagery when available.

Clue 2: An overshooting top is over the station (VIS and IR).

High resolution visible imagery is most useful for finding overshooting tops. Overshooting tops are a result of strong vertical motion that causes a thunderstorm to penetrate the anvil or the tropopause. Several such cases have been documented by Fujita (1972), Shenk (1974), and others. Locally severe weather, including heavy rainfall, has been associated with overshooting tops.

An example of overshooting tops is shown at (A) in the high resolution visible imagery in figure 10-a. An enhanced IR picture for the same time is shown in figure 10-b. Overshooting tops are more easily recognized in the higher resolution visible pictures than in IR imagery. In figure 10-a, overshooting tops are embedded in the anvil debris over eastern Iowa and Wisconsin. One of these shows up at (T) in the IR picture as an isolated colder area of Cbs embedded in the anvil debris produced by the storms over Iowa. In figure 9-b, the convective clouds in the visible picture are quite textured and have overshooting tops near the center (A) of the Cb system. This coincides with the coldest temperatures in the matching IR picture (figure 9-a); heavier rainfall would be expected near this center.

Clue 3: Anvil is brighter and/or more textured at station end of anvil (VIS).

Studies by Woodley, et al. (1972) and Griffith, et al. (1976) have shown that the brighter the cloud in visible pictures, the heavier the rainfall. Bright-textured clouds usually indicate the location of the active areas in a convective system; darker or smoother clouds usually represent areas of little or no rainfall. An example which contrasts the dark-smoother clouds (B) with bright-textured ones (A) is shown in figure 11-a. Radar data for the same time is given in figure 11-b. Note that the heavy rain extends through the brightest and textured portion of the cloud and little or no rainfall is associated with the smooth, darker translucent anvil. This storm system produced extensive flooding in portions of the Chicago area.

Clue 4: From comparing last two pictures, station is under half of anvil bounded by edge which moves least (IR).

Two successive IR pictures are compared to determine if the station is under the upwind half of the anvil. That portion of the anvil which moves least is over the slower moving core and therefore is the most active and contains the
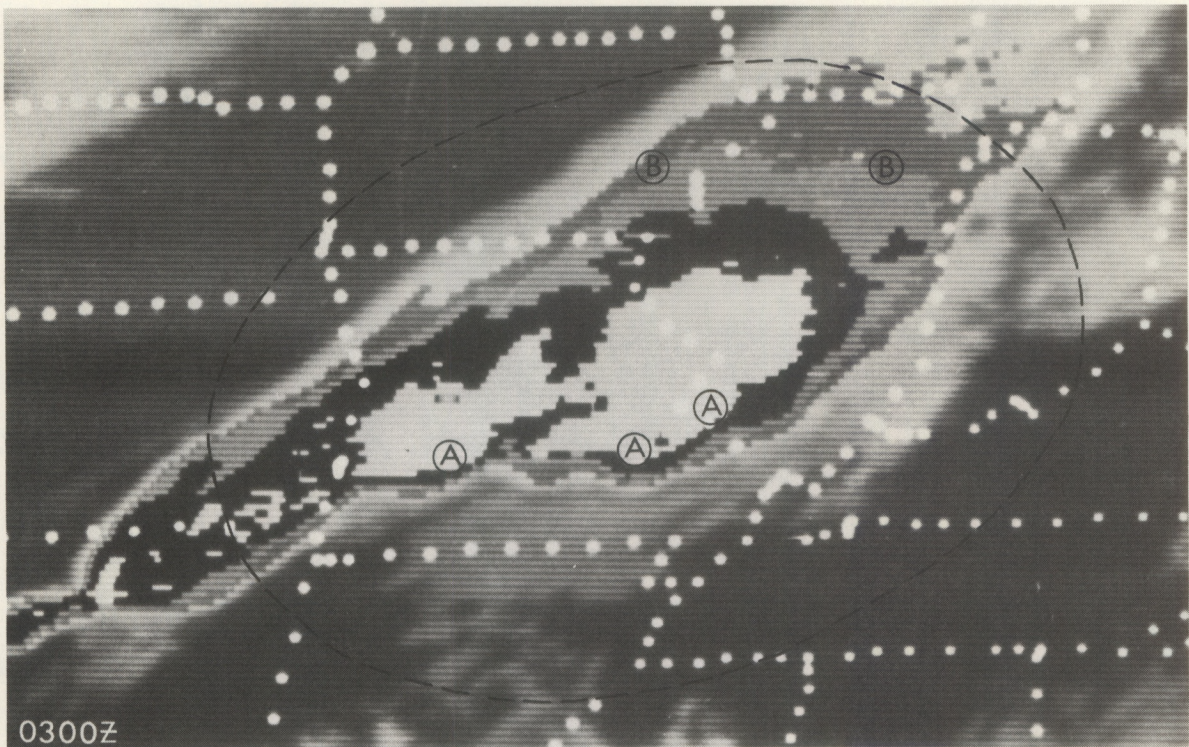
Figure 6a.--Enlarged area from full disk IR image displayed using analog enhancement, 0300 GMT, 26 August 1975.
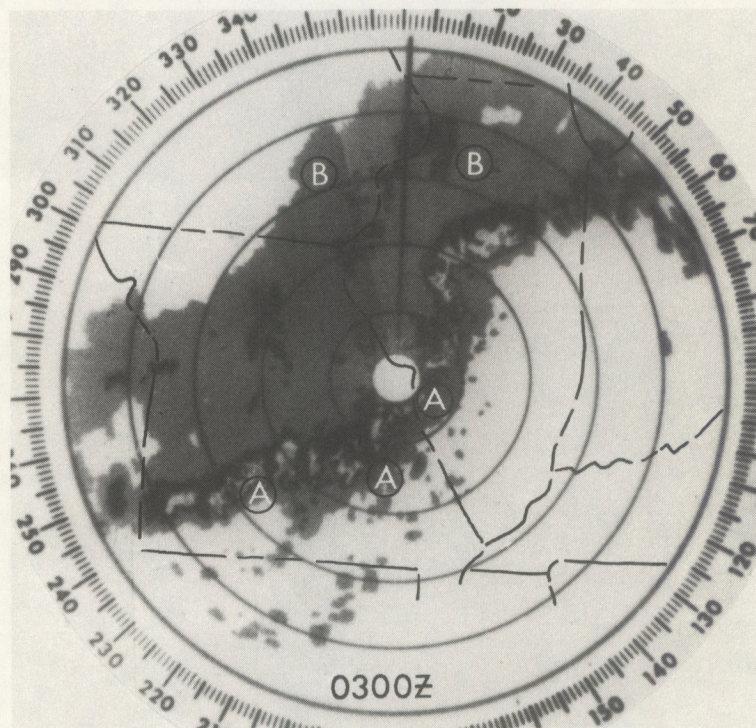

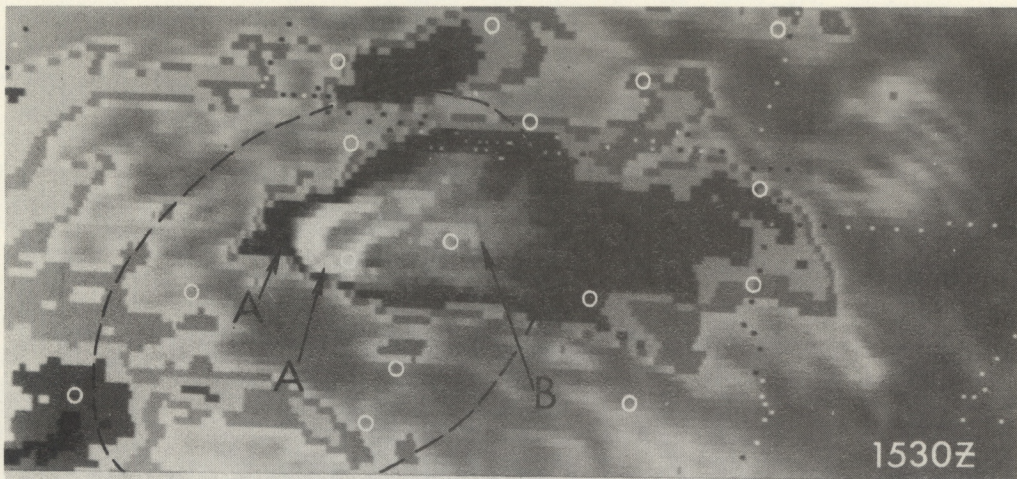Figure 6b.--Radar picture from St. Louis, Missouri, 0300 GMT, 26 August 1975.

13

Figure 7a.--Enlarged area from 2-km equivalent IR produced using digital enhancement (Mb curve), 1530 GMT, 25 May 1976.
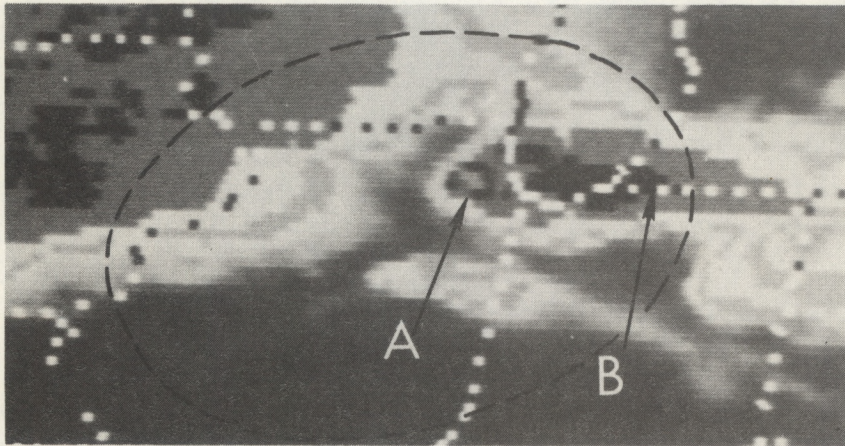

Figure 8a.--Enlarged area from 4-km equivalent IR produced using digital enhancement (Cb curve), 2345 GMT, 13 June 1976.
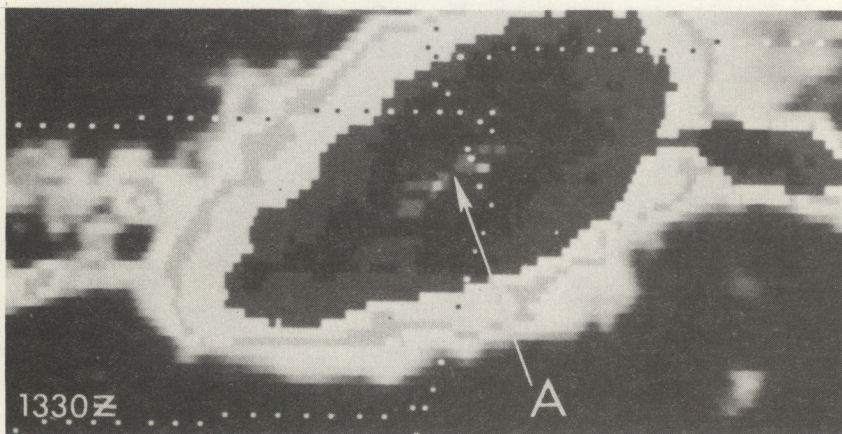

Figure 9a.--Enlarged area from 2-km equivalent IR produced using digital enhancement (Mb curve), 1330 GMT, 28 June 1976.
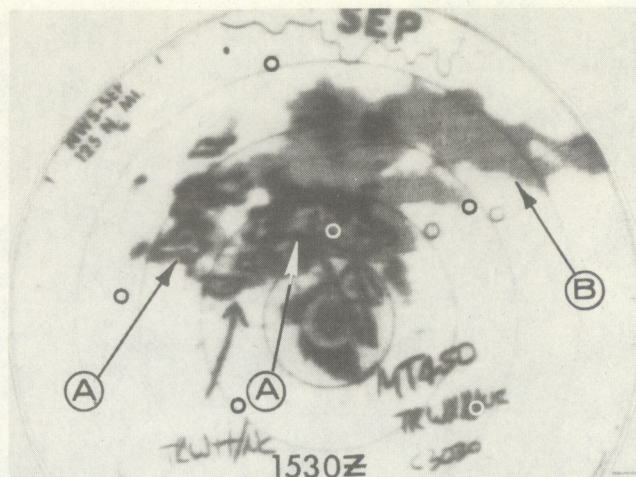
Figure 7b.--Radar picture from Stephensville, Texas,
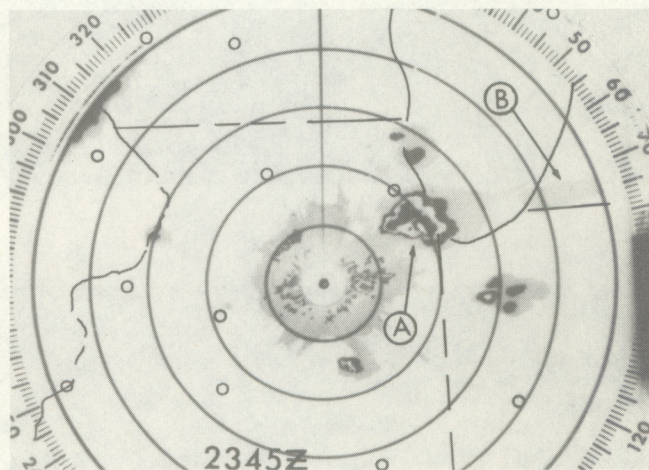1530 GMT, 25 May 1976.

Figure 8b.--Radar picture from Marseilles, Illinois,
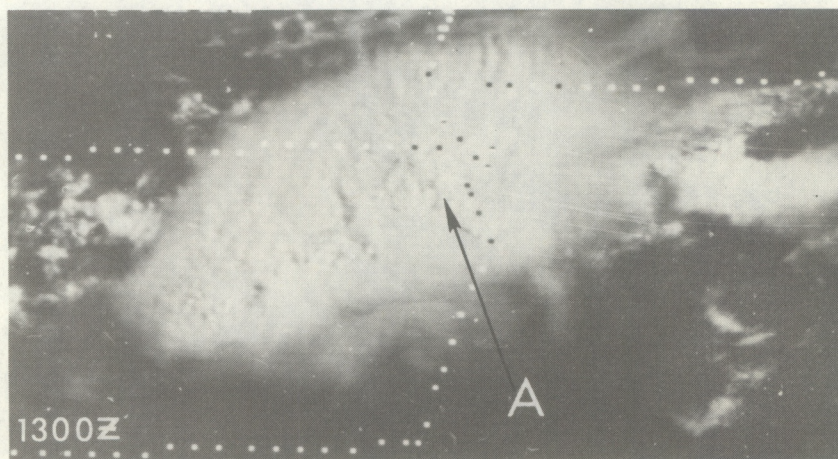2345 GMT, 13 June 1976.

Figure 9b.--Enlarged area from 2-km visible imagery,
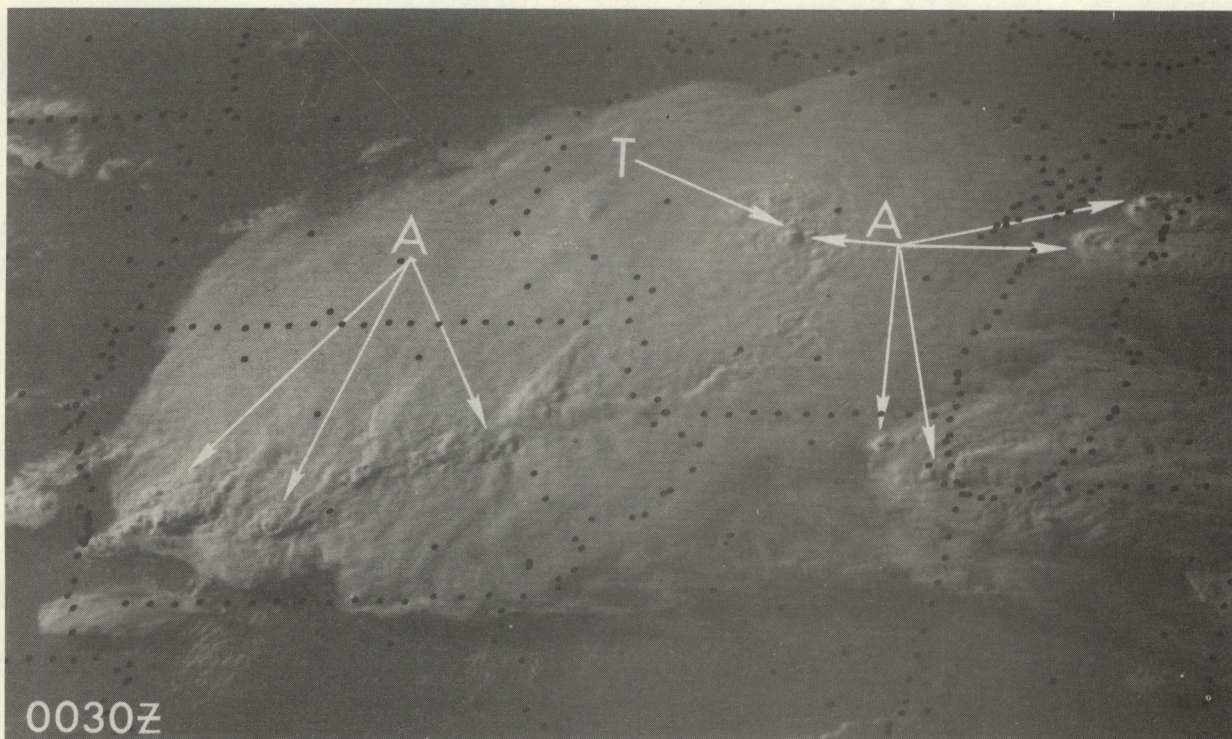1300 GMT, 28 June 1976.

15

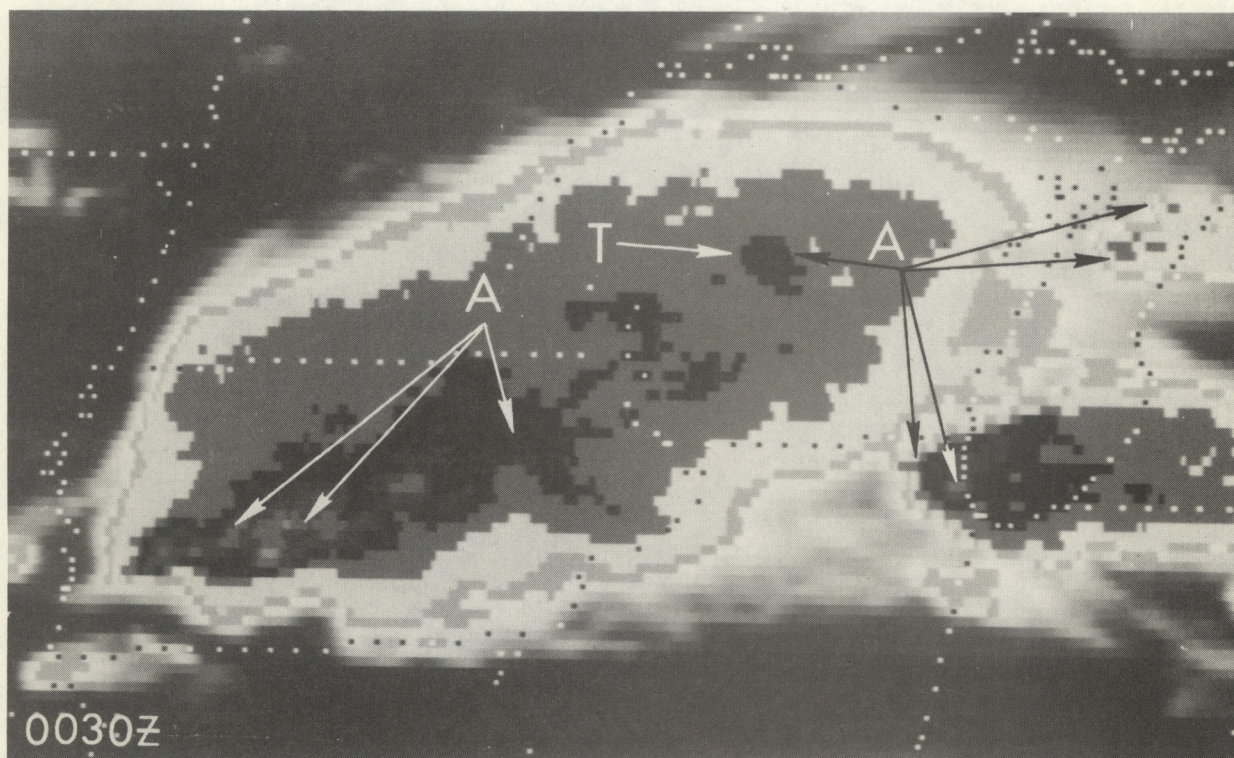Figure 10a.--One-km visible imagery, 0030 GMT, 14 June 1976.

Figure 10b.--Enlarged area from 2-km equivalent IR produced using digital enhancement (Mb curve), 0030 GMT, 14 June 1976.
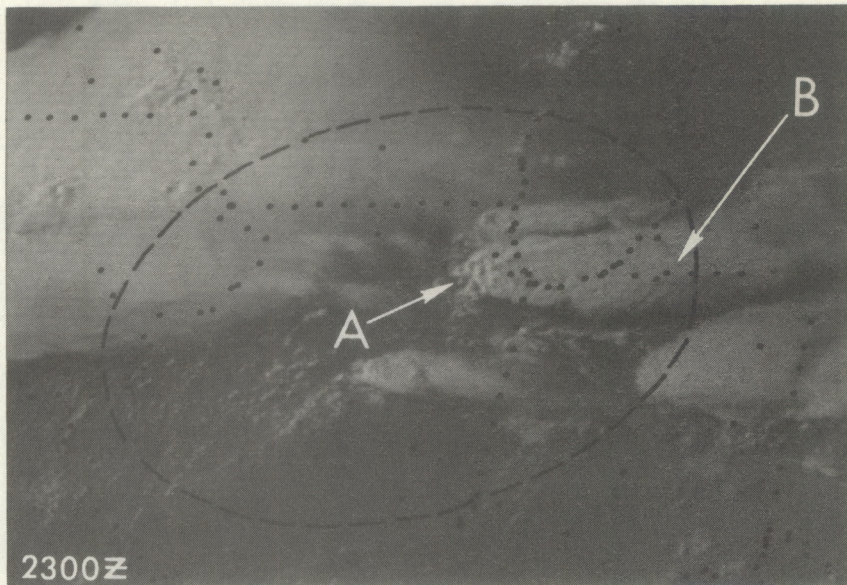
16

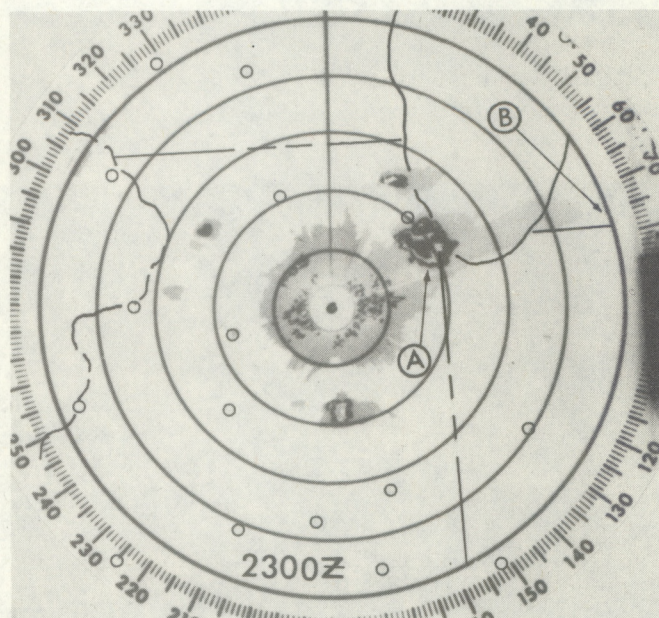Figure 11a.--One-km visible imagery, 2300 GMT, 13 June 1976.

Figure 11b.--Radar picture from Marseilles, Illinois,
2300 GMT, 13 June 1976.

significant rainfall; little or no rainfall occurs with the more rapidly
moving portion of the anvil spreading out downwind. An example contrasting
the quasi-stationary active anvil from the inactive anvil spreading out down-
wind is shown in figures 12-a and 12-b. At 1900 GMT, the western extremity
of the Cb system over Iowa at (A) is indicated by (L) and the eastern extremity
by (L'). By 1930 GMT, the western extremity at (L) has moved little and is
active while the eastern extremity is inactive and has moved rapidly downwind
as compared to its location 30 minutes earlier at (L').
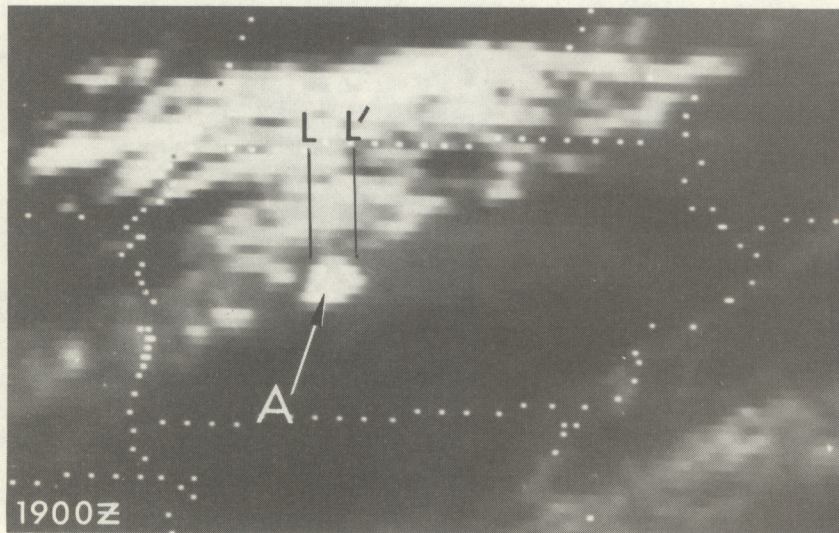

Figure 12a.--Enlarged area from 2-km equivalent IR produced using digital
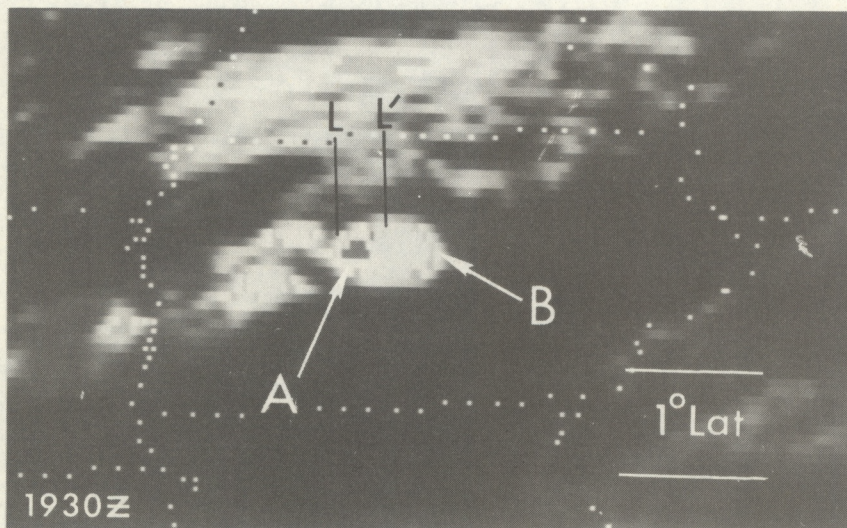enhancement (Mb curve), 1900 GMT, 13 June 1976.

Figure 12b.--Enlarged area from 2-km equivalent IR produced using digital
enhancement (Mb curve), 1930 GMT, 13 June 1976.

18

Clue 5: Station is near the 300 mb upwind end of anvil (IR).

The observed winds aloft, usually best at 300 mb, are used for determining the upwind end of the anvil. The following example illustrates the use of upper level winds for locating the upwind-active end of the anvil. At 1200 GMT, 13 June 1976, the 300 mb wind analysis in figure 13 shows 65-knot WSW winds over Iowa. For the Cb system over Iowa at 1930 GMT in figure 12-b, the upwind-active end of the anvil, according to the 300 mb wind analysis, would be at (A) while (B) locates the 300 mb downwind-inactive end of anvil. Determining the upwind-downwind end of the anvil from upper air data is particularly useful at those stations which receive satellite imagery less frequently, e.g., twice a day.

From using the above clues as guidelines in the analysis of the satellite pictures, the decision is made as to whether or not the station is under the active portion of the convective system. If the station is not under the active portion, the estimate is 0.01 inches of rain (enter in Total Estimate Box of Step 6 on page 32). If the station is under the active portion, proceed to Step 4.
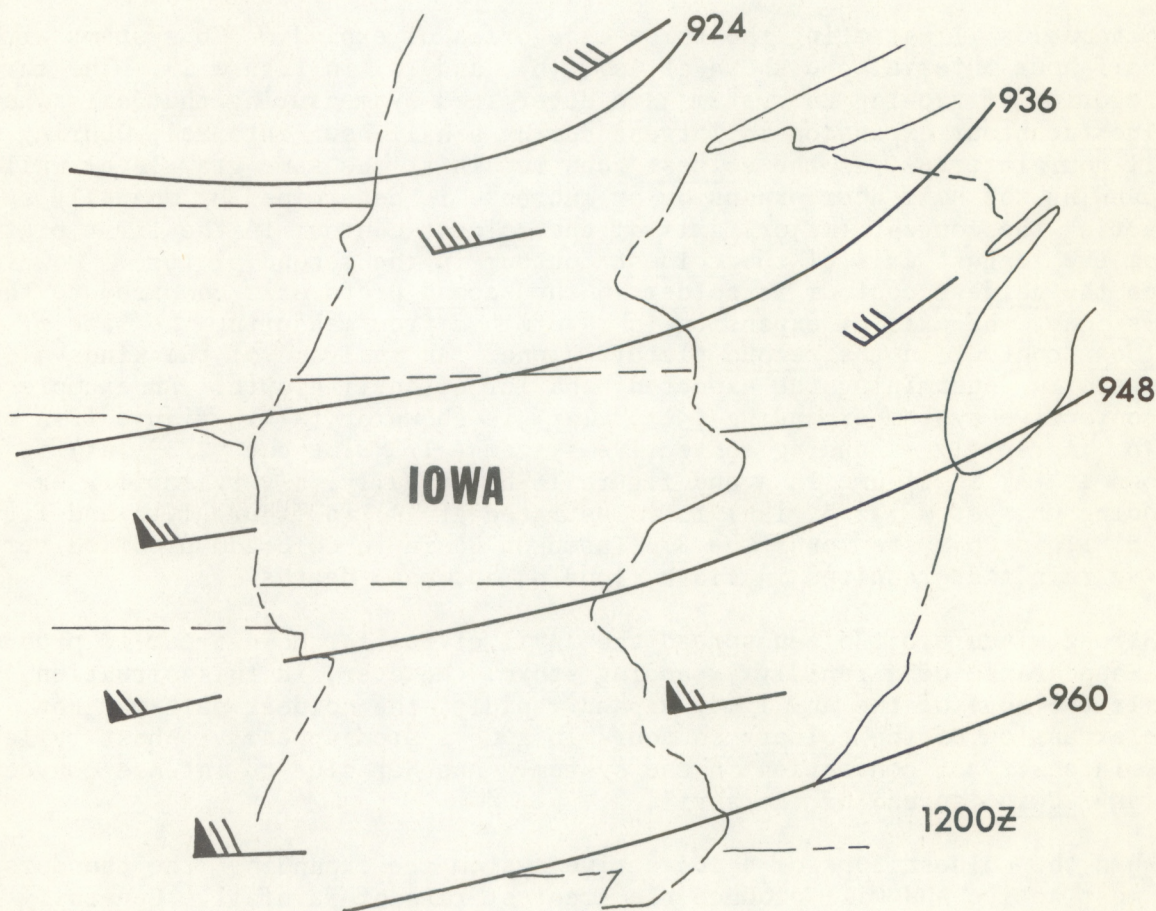

Figure 13.--300 Mb Analysis, 1200 GMT, 13 June 1976.

19

Figure 14:   Step 4 of the Decision Tree.

In this step a first guess estimate of the rainfall is obtained from the enhanced IR alone. Half-hourly rainfall rates are estimated as a function of cloud top temperature and ongoing temperature changes in consecutive half-hourly enhanced IR pictures. The rainfall rates are obtained by determining: (1) the cloud-top temperature over the station at the time of the second picture and (2) the half-hourly change in the coldest cloud tops of the Cb system affecting the station. If the highest cloud tops are colder in the second picture as compared to the first one, the expansion rate is determined from the observed size of the coldest contour in the second picture alone. The expansion of the coldest contour (whether it be in the first and second pictures or in the second picture alone) appears to be best related to the intensity of the convection. Knowledge of (2) allows the following question to be answered. Did the area of coldest tops expand, remain the same, or contract and become warmer during the half-hour interval? The coldest tops of the Cb system determine the categories (expanding, remaining the same, contracting) to be used in this step of the estimate. When expansion occurs, decide if the coldest tops increased in length along their axes by less than one-third of a degree of latitude, between one-third and two-thirds of a degree, or more than two-thirds of a degree within a half-hour.

Schematics illustrating the three categories of expanding Cb systems within a half-hour interval are shown at (a), (b), and (c) in figure 15. The three categories of growing Cb systems are determined by measuring that axis where coldest contour expansion is largest during a half-hour interval. During a half-hour interval, if the coldest tops remain at the same gray level while expanding, the half-hour expansion or increase is determined by mentally sub-tracting the longest (major) axis of the coldest contour in the first picture from the longest axis of the coldest contour in the second picture. However, when the coldest contour is colder in the second picture as compared to the first one, the axis of expansion is determined from measuring the size of the coldest contour in the second picture alone. An analysis of the winds aloft can aid in determining the expected behavior of anvil growth. An example of a convective system expanding ($\leq 1/3^{\circ}$ lat) is shown at (A) in figure 12-a and 12-b. A rapidly expanding convective system ($>1/3^{\circ}$ lat but $\leq 2/3^{\circ}$ lat) is shown at (A) in figure 16-a and figure 16-b. Finally, a very rapidly expanding Cb system ($>2/3^{\circ}$ lat) is illustrated at (A) in figure 17-a and figure 17-b. This Cb system over the Big Thompson Basin in Colorado produced very heavy rain that resulted in flash flooding and many deaths.

Strong winds aloft often spread the anvil cirrus far downstream to produce the appearance of a rapidly expanding storm. However, in this situation, while the edge of the anvil may expand rapidly, the coldest part may not. The expansion of the coldest contours in a Cb system appears to best reflect the intensity of convection in the system. Another clue to intense convection is any upwind spread of the anvil.

When the coldest tops of a convective system are expanding, the thunderstorm is most active and will produce the greatest rate of rainfall. Generally, the more rapid the expansion, the heavier the rainfall.
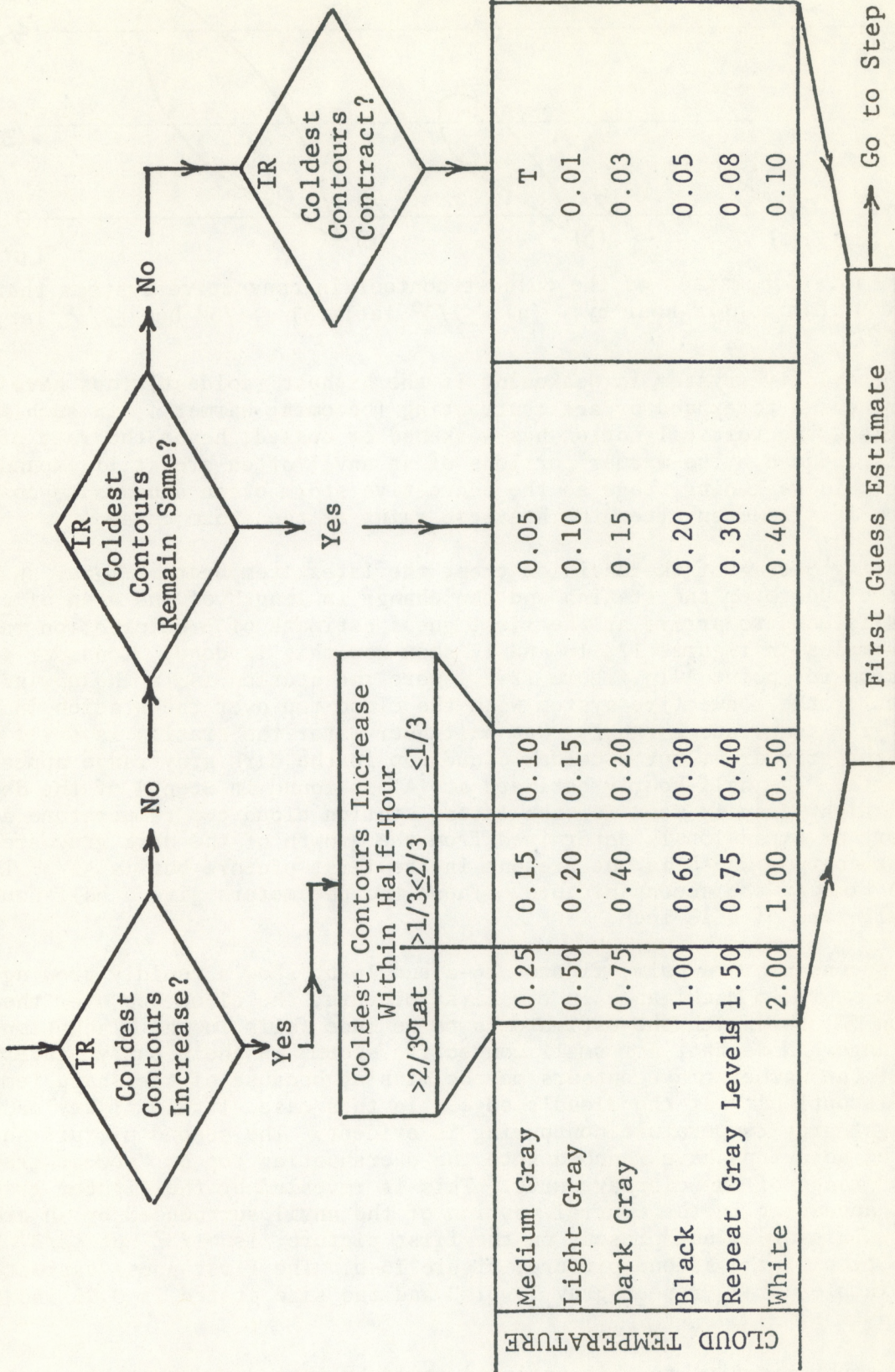
STEP 4

IR Coldest Contours Increase? → Yes / No

No → IR Coldest Contours Remain Same? → Yes / No

No → IR Coldest Contours Contract?

CLOUD TEMPERATURE	Coldest Contours Increase Within Half-Hour			Yes	T
	>2/3°Lat	>1/3 ≤2/3	≤1/3		
Medium Gray	0.25	0.15	0.10	0.05	T
Light Gray	0.50	0.20	0.15	0.10	0.01
Dark Gray	0.75	0.40	0.20	0.15	0.03
Black	1.00	0.60	0.30	0.20	0.05
Repeat Gray Levels	1.50	0.75	0.40	0.30	0.08
White	2.00	1.00	0.50	0.40	0.10

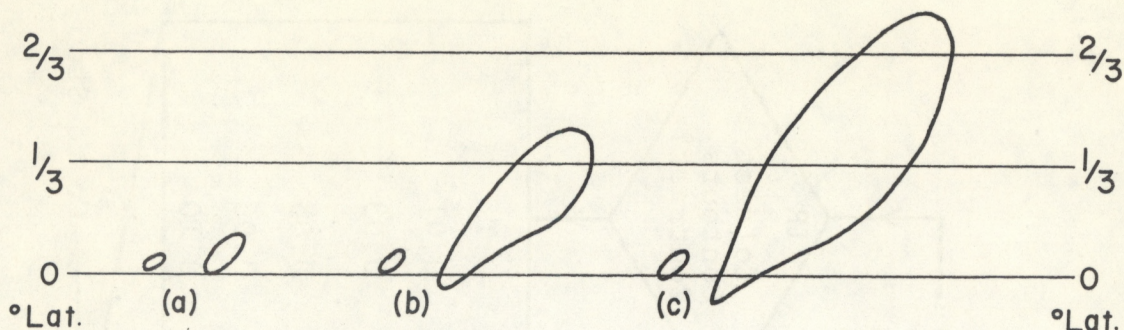First Guess Estimate → Go to Step 5

Figure 14.--Step 4 of the Decision Tree.

21

Figure 15.--Schematics of the coldest contour in convective systems that expand within a half-hour by: (a) $\leq 1/3^o$ lat; (b) $>1/3^o$ but $\leq 2/3^o$ lat; (c) $>2/3^o$ lat.

The convective system is weakening if the highest (coldest) tops have either ceased to expand or are contracting (becoming warmer). In such a situation, the vertical motion has weakened or ceased; hence the rate of rainfall is reduced. The warmer portions of an anvil often are still expanding during this weakening stage so the convective storm often appears to continue to grow in size even after the heaviest rains of the storm cease.

In using Step 4 of the decision tree, the latest temperature (gray shade) of the clouds over the station and the change in length of the area of <u>coldest</u> clouds is used to arrive at the first guess estimate of precipitation rate. The examples in figures 12, 16 and 17 show how this is done. Consider the situation for point A in figure 12-a. Here the station is in the upwind portion of the convective system with the cloud top over the station in the light gray temperature range. One half-hour later the station is still under the light gray area, but a colder cloud top in the dark gray range appears to the north. The half-hourly estimate at (A) is found in Step 4 of the decision tree. Light gray is used for the latest station cloud top temperature and the category of expansion is determined from the growth of the dark gray area, the coldest contour which is not present in the first picture but is $\leq 1/3^o$ lat by the time of the second picture. These two parameters give a half-hourly rainfall rate of 0.15 inch.

The second picture pair, figures 16-a and 16-b, show a rapidly growing convective storm in Michigan. In the first picture, the cloud top over the station (A) for which the estimate is to be made falls in the black temperature range. Note that for small convective storms in their early stages, some of the warmer gray contours may be missing because of the sharp temperature discontinuity at the cloud's edge. In this case, little if any medium and light gray temperature contouring is evident. The second picture shows that the cold tops have reached into the overshooting top or "repeat gray levels" range of the display curve. This is revealed by the lighter gray shades appearing in the central portion of the anvil surrounded by an area of black. This area, not present on the first picture, is $>1/3^o$ but $\leq 2/3^o$ lat by the time of the second picture, figure 16-b. The first guess estimate for this example using "repeat gray levels" and the size stated is 0.75 inches of rain.

Some sophistication to this estimate could be introduced by taking into account that the station was under a black contour (0.60 inches of rain) for

part of the period and repeated gray levels (0.75 inches of rain) for the remainder, while the coldest contour expanded >1/3 but ≤2/3° lat. An average of 0.60 and 0.75 would give a half-hour rainfall rate of around 0.67 inches of rain. In this situation, there is little difference between the 0.67 and 0.75 rainfall estimate and such sophistication is not necessary in an estimating scheme. However, in an extreme case where rapidly expanding (>2/3° lat) contours over a station change from medium gray to white in a half-hour period, a more representative half-hour rainfall estimate would be the average of 0.25 inches of rain (for medium gray) and 2.00 inches of rain (for white).

The third example in figure 17-a and 17-b shows the clouds over Colorado just prior to the Big Thompson flood. In this case, the cloud top temperature over the station (indicated by A) is in the repeat gray level temperature range on the first picture and in the white level a half-hour later. Therefore, the area of white in the second picture is measured to determine the coldest cloud top increase. The first guess estimate using "white" and >2/3° lat is 2.00 inches per half-hour.

When two enhanced IR pictures show the active portion of the Cb over the station in the first picture but has moved away a half-hour later, the precipitation is estimated as follows. Rainfall occurred during the first portion of the period but none for the remainder which reduces the half-hour rate by approximately 50 percent.

When the coldest tops remain the same, usually the convective activity has peaked resulting in lesser amounts of rain. An example of a convective system whose coldest tops practically remain the same is shown at (A) in figure 18-a and figure 18-b. The half-hour rainfall estimate using "dark gray" at (A) is 0.15 inches.

When the coldest tops are contracting (becoming warmer) or the anvil has become detached from its roots, the convective system has dissipated; there will be little or no additional rainfall. An example of a convective system contracting is shown at (A) in figure 19-a and figure 19-b. The half-hour rainfall estimate using "dark gray" at (A) is 0.03 inches.

The rainfall estimates from Step 4 are entered into the "First Guess Estimate" box in Step 6 on page 32. Now proceed to Step 5.

Figure 20: Step 5 of the Decision Tree.

This step is used to analyze the imagery for the presence of precipitation amplifiers not always accounted for in the First Guess by determining if overshooting tops, merging thunderstorms, or merging convective cloud lines appeared during the past half-hour in the visible or IR imagery. These precipitation amplifiers are more easily recognized in the high resolution visible imagery.

Overshooting tops were discussed previously and examples were shown in figures 9 and 10. If overshooting tops occurred over the station in the first or second picture of a half-hour interval picture pair, 0.50 or more inches of rain is added to the "First Guess Estimate." If only hourly pictures are
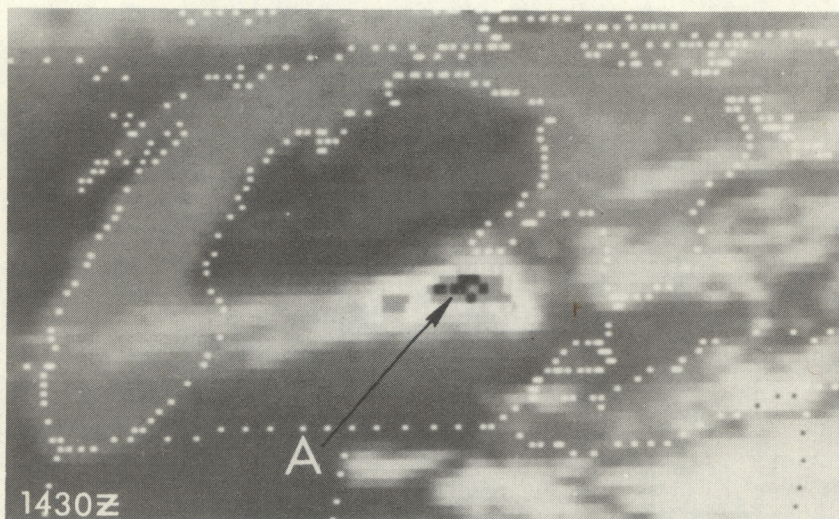
23

Figure 16a.--Enlarged area from 2-km equivalent IR produced using digital enhancement (Mb curve), 1430 GMT, 11 July 1976.
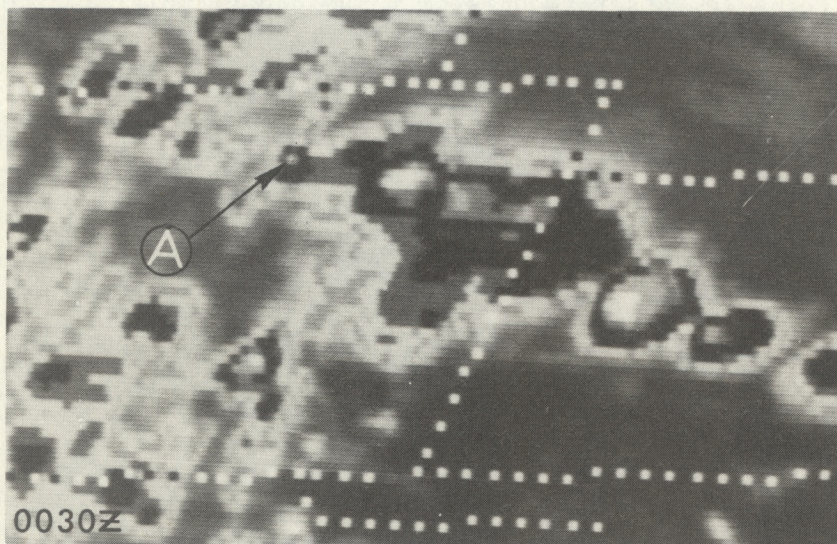

Figure 17a.--Enlarged area from 4-km equivalent IR produced using digital enhancement (Cb curve), 0030 GMT, 1 August 1976.
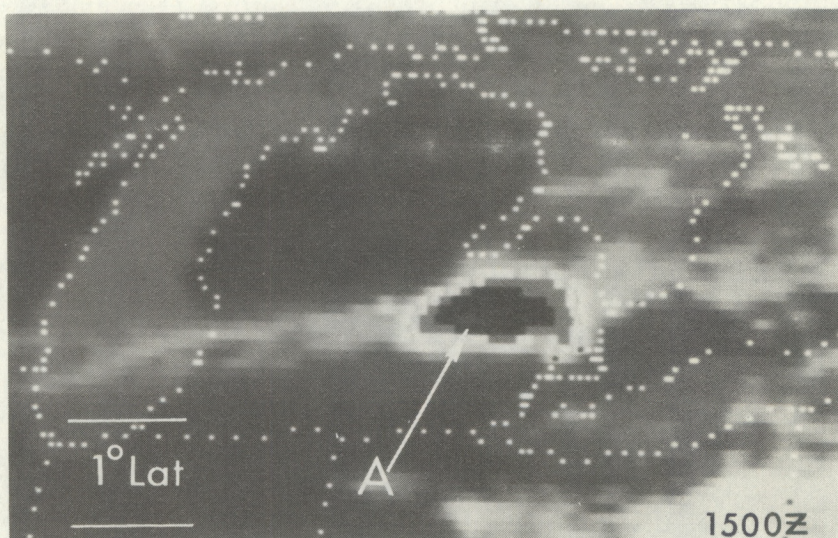
Figure 16b.--Enlarged area from 2-km equivalent IR produced using digital enhancement (Mb curve), 1500 GMT, 11 July 1976.
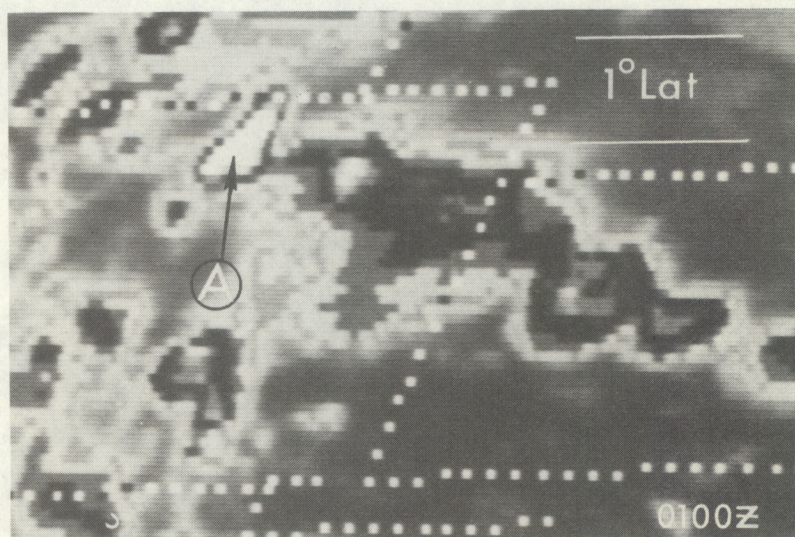

Figure 17b.--Enlarged area from 4-km equivalent IR produced using digital enhancement (Cb curve), 0100 GMT, 1 August 1976.

available, the additive factor should remain at around 0.50 inches per half-hour. However, when the analyst has confidence that the overshooting tops continued throughout the one-hour period, one inch of rain should be added to the estimate.

Merging convective cloud lines over a station increase the rainfall rate. High resolution visible and IR pictures in figures 21-a and 21-b, respectively, show a north-south cloud line with embedded thunderstorms at (A) merging with a sea breeze cloud line at (B-B'). The lines merge near Houston, Texas, where a very heavy rainfall occurred during the period 1700 to 0100 GMT, June 15-16, 1976. Six-hour rainfall amounts of near 13 inches were reported with this system. In figure 21, the convective cloud line at (A) merging into the thunderstorm system near Houston at (C) represents a convergent zone in which
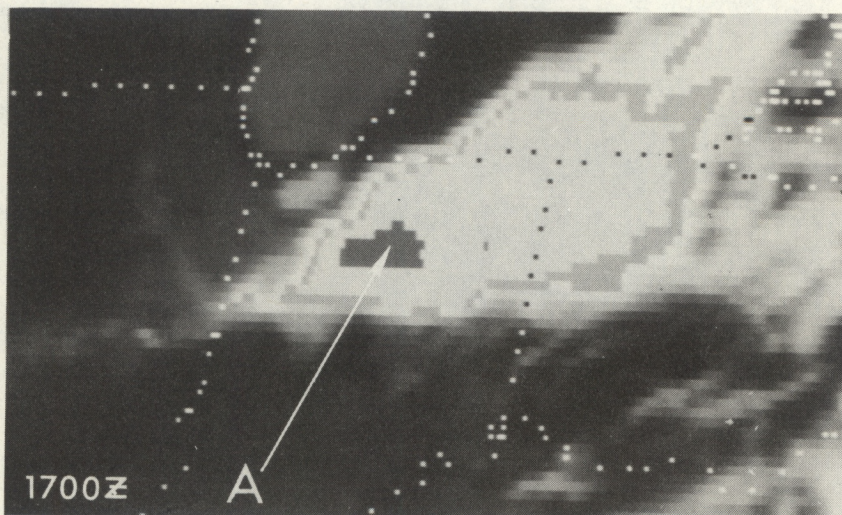

Figure 18a.--Enlarged area from 2-km equivalent IR produced using digital enhancement (Mb curve), 1700 GMT, 13 June 1976.
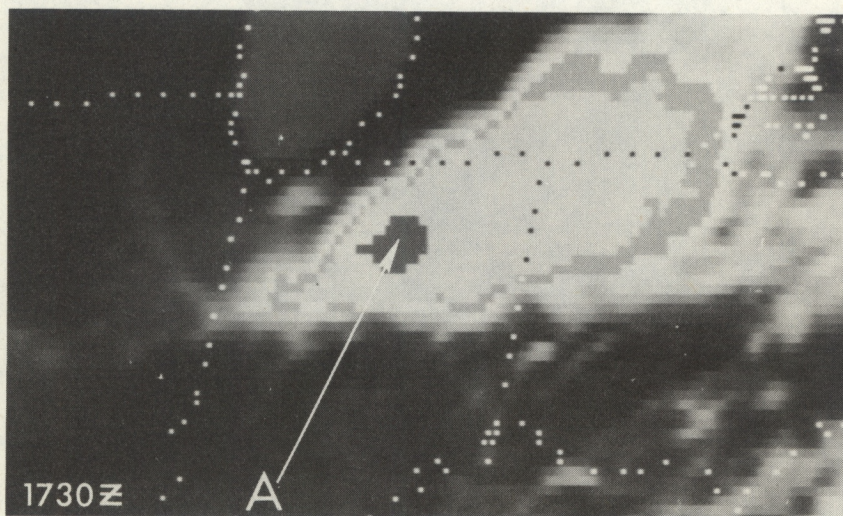

Figure 18b.--Enlarged area from 2-km equivalent IR produced using digital enhancement (Mb curve), 1730 GMT, 13 June 1976.

additional low level moisture is concentrated. This convergence results in nearly continuous merging of the storms where the two lines meet and causes heavier rainfall than that accounted for in the "First Guess" part of the decision tree. Therefore, an additional 0.50 inches or more of rain is added to the "First Guess" rainfall estimate for those areas affected by the merging convective cloud lines observed in the first or second picture of a half-hour interval picture pair. This factor of 0.50 inches per half-hour is added as long as the merging convective cloud lines are maintained over the area. If only hourly pictures are available, the additive factor should remain 0.50 unless the convective cloud line merger continues for the entire hour; for one-hour "merging situations," one or more inches of rain should be added.
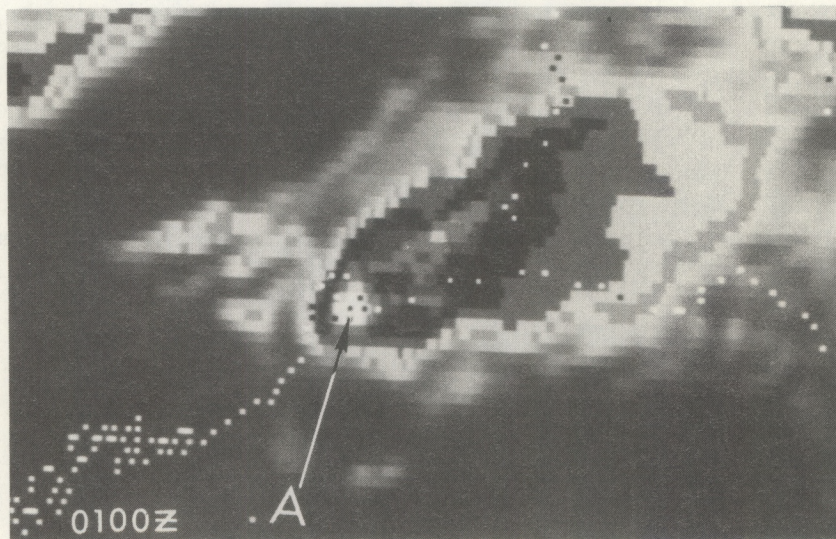

Figure 19a.--Enlarged area from 2-km equivalent IR produced using digital enhancement (Mb curve), 0100 GMT, 16 June 1976.
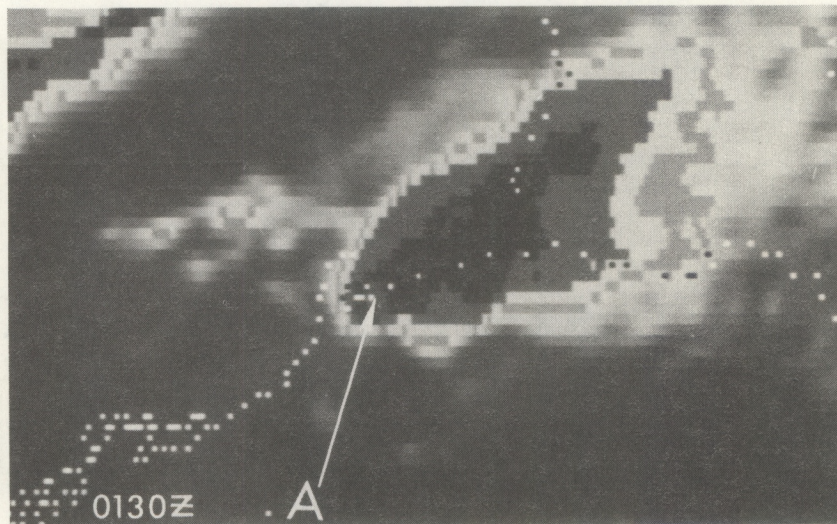

Figure 19b.--Enlarged area from 2-km equivalent IR produced using digital enhancement (Mb curve), 0130 GMT, 16 June 1976.

Thunderstorm mergers as established by Simpson and Woodley (1971) and Woodley and Sax (1976) have the dramatic effect of greatly increasing rainfall. If thunderstorms merged during the half-hour period, then 0.50 inches or more of rain is added to the "First Guess Estimate." The merger must be occurring at the station for the station to be affected. There is evidence that some Cb mergers enhance the rainfall substantially more than the suggested 0.50 inches and account for many of the observed flash flooding situations. Enhanced IR and high resolution visible views of merging thunderstorm lines or cells are displayed in figures 22-a through 22-d and 23-a through 23-d, respectively. In figures 22-a, and 22-b, and 23-a and 23-b, (A-A'), (B-B'), (C-C') locate three initial thunderstorm lines; the merger point of lines (A-A') and (B-B') is located at (M) in figures 22-c and 23-c. Between 2230 GMT and 2300 GMT, an additional merger takes place between the thunderstorm line (C-C') and the storms at (M). The result is a large, intense thunderstorm area located at (M') in figures 22-d and 23-d. Because of the poorer resolution of the IR and the obscuring effect of Cb anvils, mergers are less accurately interpreted from IR than from high resolution visible imagery. The two-km visible imagery, figures 23-c and 23-d, show that overshooting tops are produced near the area of the mergers. The IR images, figures 22-c and 22-d, illustrate development of the coldest cloud tops (white) in proximity of the mergers. Radar data from Miami showed the mergers of three separate precipitation echoes near (M) and (M') between 2200 and
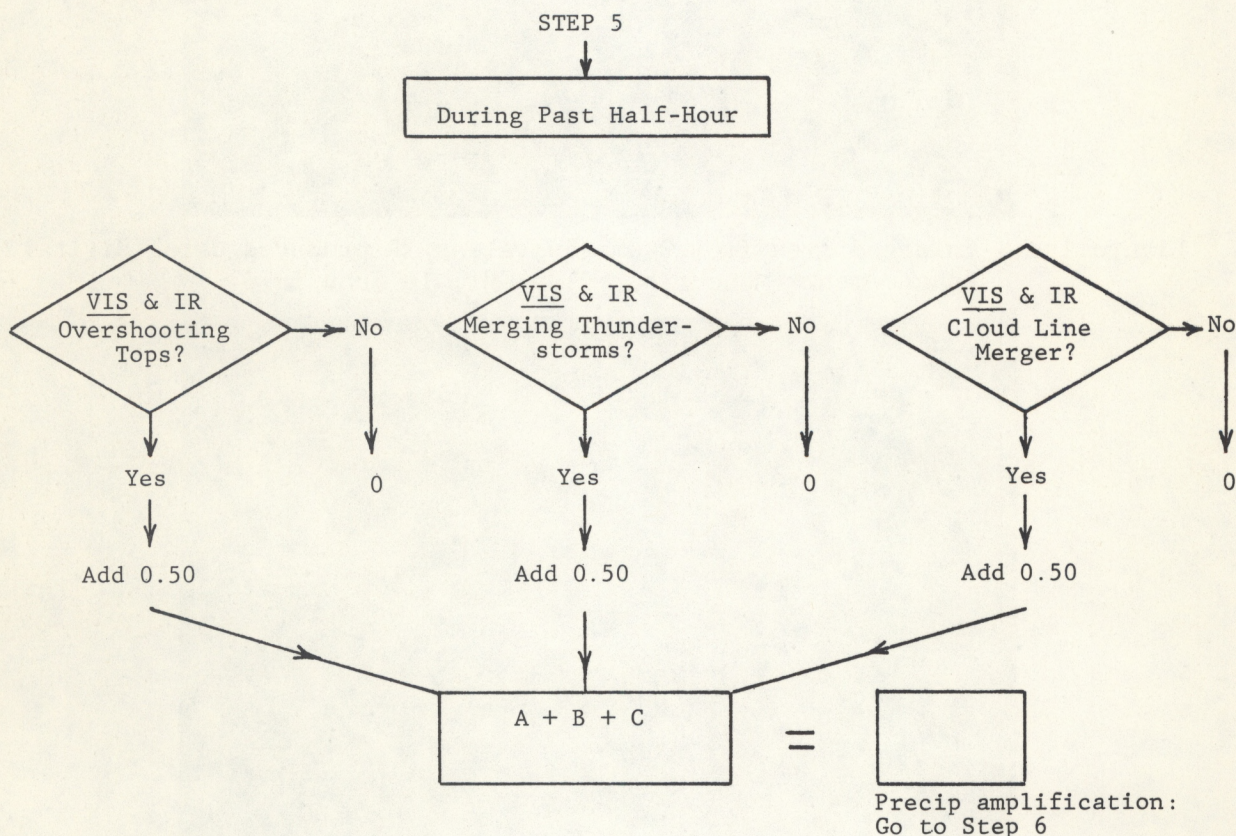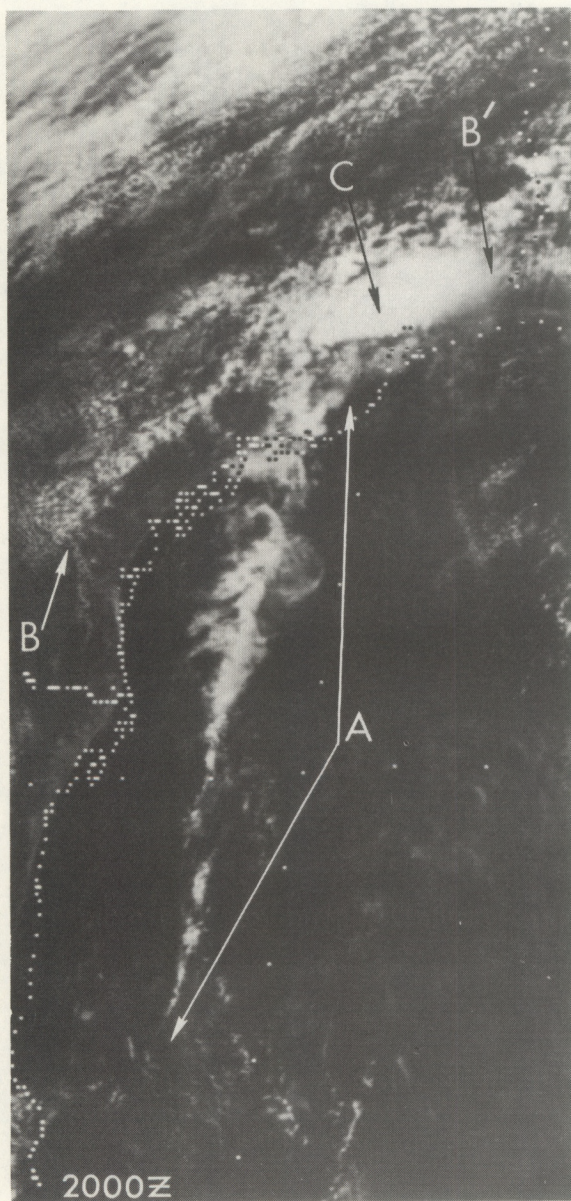
Figure 20.--Step 5 of the Decision Tree.

28

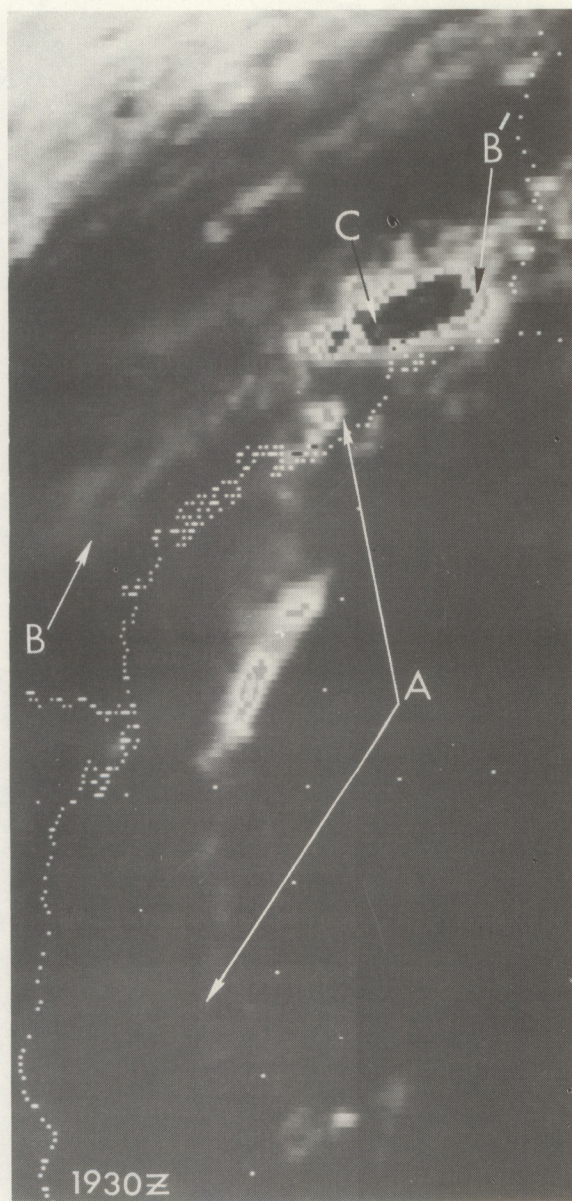Figure 21a.--Enlarged area from 2-km visible imagery, 2000 GMT, 15 Jun 76.

Figure 21b.--Enlarged area from 2-km equivalent IR produced using digital enhancement (Mb curve), 1930 GMT, 15 Jun 76.

Figure 22a.--Enlarged area from 2-km equivalent IR produced using digital enhancement (Mb curve), 2130 GMT, 21 July 1976.

Figure 22b.--Enlarged area from 2-km equivalent IR produced using digital enhancement (Mb curve), 2200 GMT, 21 July 1976.

Figure 23a.--Enlarged area from 2-km visible imagery, 2130 GMT, 21 Jul 76.

Figure 23b.--Enlarged area from 2-km visible imagery, 2200 GMT, 21 Jul 76.
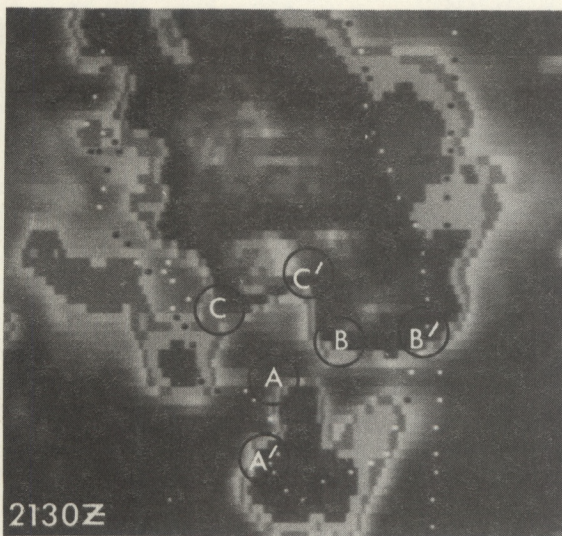
30

Figure 22c.--Enlarged area from 2-km
equivalent IR produced using digital
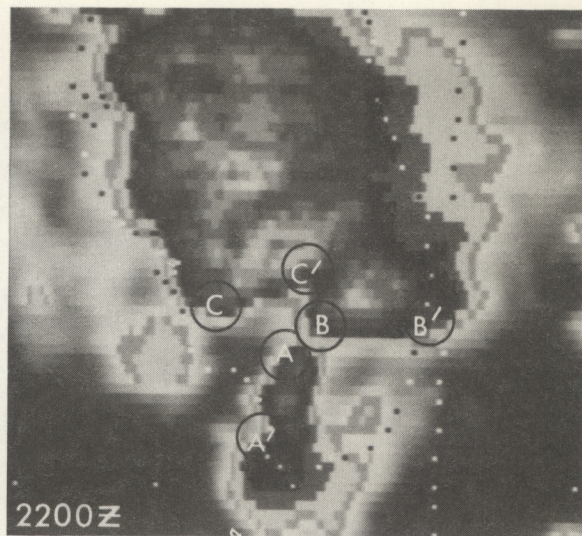enhancement (Mb curve), 2230 GMT,
21 July 1976.

Figure 22d.--Enlarged area from 2-km
equivalent IR produced using digital
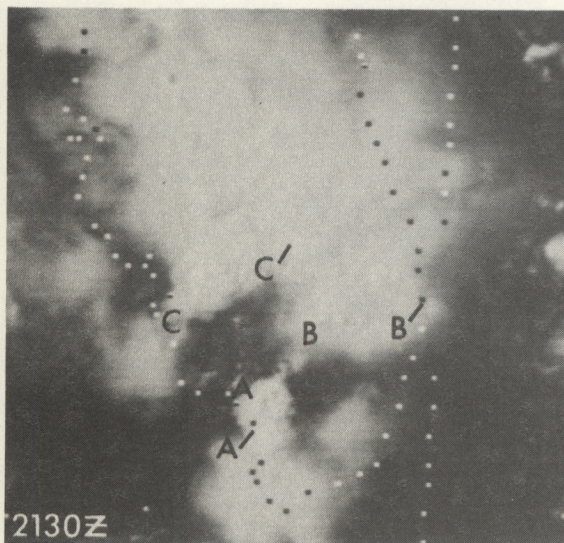enhancement (Mb curve), 2300 GMT,
21 July 1976.

Figure 23c.--Enlarged area from 2-km
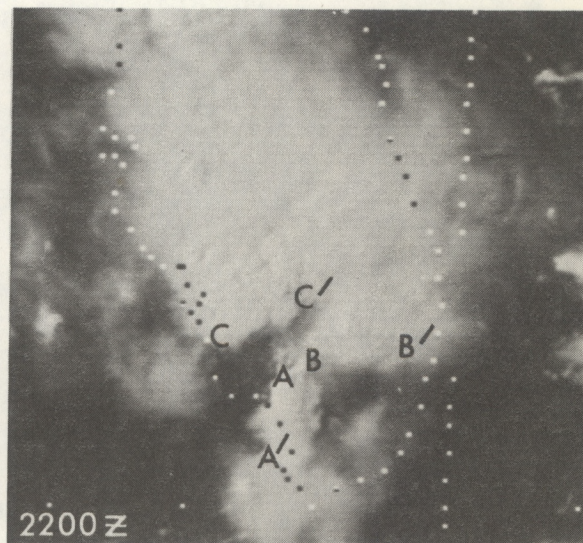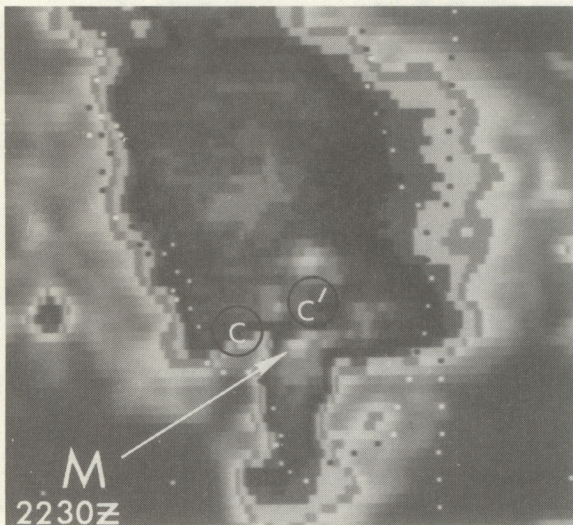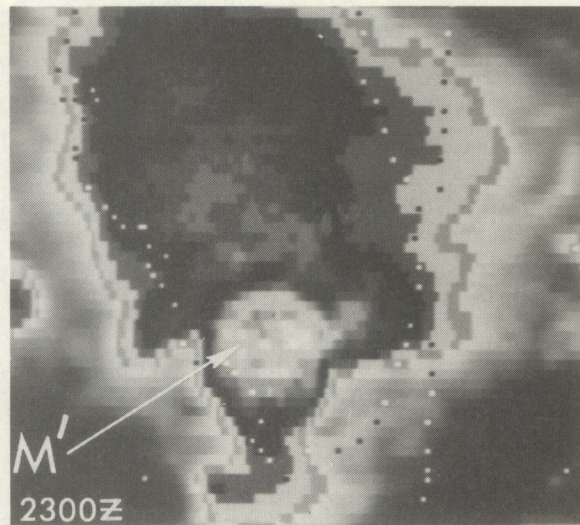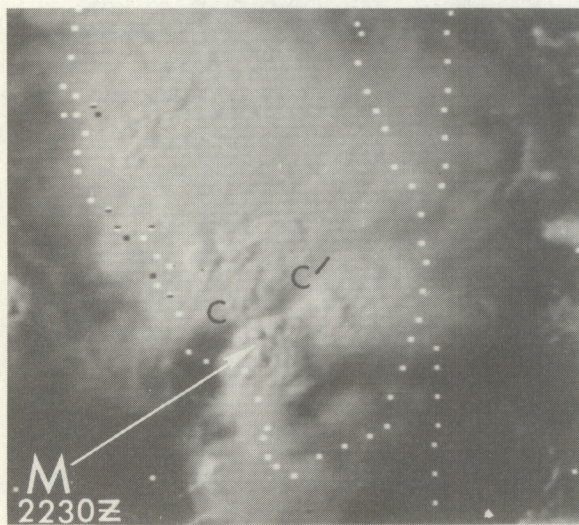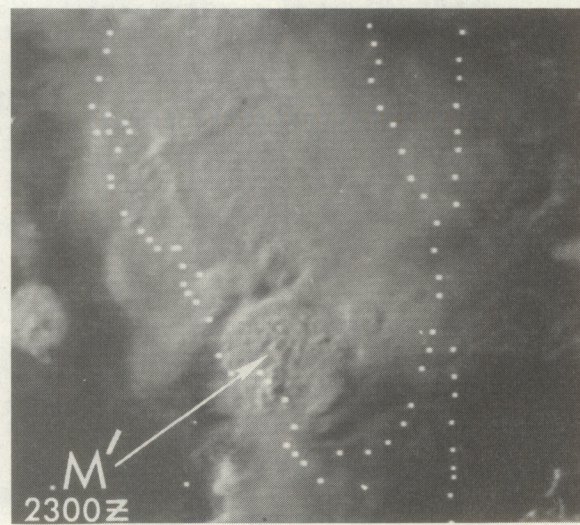visible imagery, 2230 GMT, 21 Jul 76.

Figure 23d.--Enlarged area from 2-km
visible imagery, 2300 GMT, 21 Jul 76.

31

2230 GMT and 2230 and 2300 GMT in figures 22-c and 22-d, and 23-c and 23-d. The mergers caused an increase in areal coverage and intensity of the precipitation echoes. If only hourly pictures are available, the additive factor should still be around 0.50 inches unless there is evidence that more than one merger occurred during the one-hour period. For situations in which such additional merging is indicated, one inch of rain should be added to the estimate.

The rainfall estimations arrived at by consideration of these precipitation amplifiers are summed and entered into the "Precipitation Amplification" box in Step 6.

Figure 24: Step 6 of the Decision Tree.

In this final step, the total rainfall estimate is calculated by summing the "First Guess" from Step 4 and the "Precipitation Amplification" amount from Step 5. Rainfall estimates obtained from Steps 2 and 3 are entered directly into the Total Estimate.

At many stations only hourly enhanced IR pictures are received. The scheme can still be used by comparing the ongoing changes in consecutive one-hour pictures. However, the decision tree has to be modified as follows: (1) For Cb systems that remain the same or are contracting, the half-hour values from the decision tree are doubled to obtain a one-hour estimate; (2) For Cb systems that are expanding, it is not necessary to double the rainfall rate because the anvil expansion will be greater (about twice as big) and take care of the extra time. For example, the hourly estimate for a station under the coldest contour (black, -60 to -66°C) of a Cb system that expanded >2/3° lat in a one-hour period is one inch. Normally in the case of hourly pictures, the expansion rate is best determined by measuring how much the coldest contour, observed in the first picture, grew during the one-hour interval.

The complete decision tree with a brief explanation of each step is presented in the appendix.
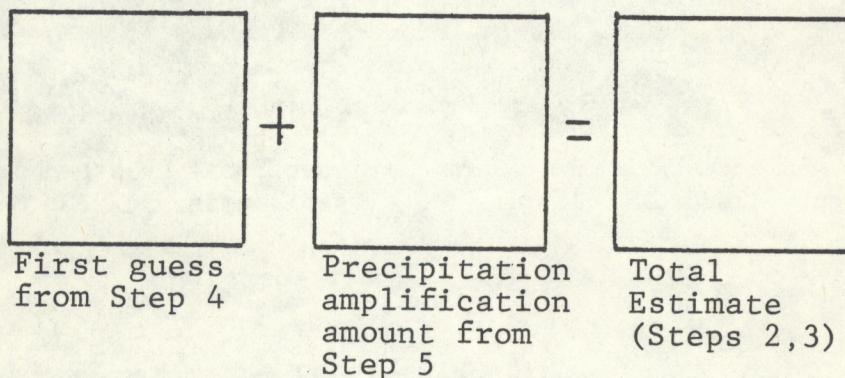
STEP 6

First guess
from Step 4

+

Precipitation
amplification
amount from
Step 5

=

Total
Estimate
(Steps 2,3)

Figure 24.--Step 6 of the Decision Tree.

III. A 24-HOUR RAINFALL ESTIMATE OF A
CONVECTIVE SYSTEM OVER IOWA

In the following example, enhanced IR and high resolution visible imagery
are used for estimating the locally heavy rainfall from a convective storm
over Iowa. Estimates were computed every half-hour at a number of arbitrary
points (40) over Iowa for a 24-hour period. The results are compared with
the observed accumulations and available radar data. A 24-hour period is
used since there are more 24-hour observations of rainfall accumulation
available than for shorter time periods. Thunderstorms of varying intensity
were present over Iowa for almost 18 hours between 1800 GMT, 13 June 1976,
and 1200 GMT, 14 June 1976.

The following estimates were computed by a meteorologist, assigned to the
Applications Group for the summer, who was given two hours of training on
using the "decision tree." He was totally unfamiliar with the rainfall over
Iowa for which the estimations were made. His half-hour estimates between
2000-2030 GMT and 2030-2100 GMT, using the enhanced IR and one-mile visible
imagery in figures 25-27, are shown in figures 26-c and 27-c. In the
satellite imagery, the X's locating Omaha, Nebraska, and Des Moines, Iowa,
are indicated by (O) and (D), respectively. An operational radar analysis
over this area for 2035 GMT, 13 June 1976, is presented in figure 28-a
and the rainfall estimated from the manually digitized radar data for 2050 GMT
is shown in figure 28-b. A comparison of the radar analysis in figure 28-a
with the half-hourly estimates of figures 26-c and 27-c shows that the
"estimated" rainfall occurs within the area of scattered intense thunderstorms
(TRWX). Also, the larger rainfall estimates in figures 26-c and 27-c, just
north of Des Moines and northeast of Omaha, are in the proximity of extreme
thunderstorm activity with tops of 54,000 and 60,000 feet, respectively. The
rainfall magnitudes and areal coverage obtained from the manually digitized
radar in figure 28-b are similar to the satellite-derived estimates in
figure 28-c (the sum of figures 26-c and 27-c). For comparison, the 24-hour
rainfall over the state (at the 40 arbitrary points) is 1.12 inches while
the observed is 1.07 inches. The average estimated 24-hour rainfall in the
area of observed heavy accumulations from near (A) in figure 29-a to just
north of Omaha is 2.18 inches; the average observed in figure 29-b is 1.50
inches. Rainfall in this area of heavier precipitation is overestimated by
45%. The main reason for these errors was the inability to distinguish
between the upwind and downwind portions of the convective system after
several Cbs had merged. In figure 29, locations near (A) were in the upwind
portion for a while but probably not as long as surmised by the meteorologist.
Locations near (B) had Cb clusters embedded within the anvil material and was
in the upwind portion for a greater period of time than analyzed by the
meteorologist. Because of the presence of the anvil cirrus, embedded Cb
clusters near (B) were virtually impossible to detect in the IR. Much of
the rainfall near (B) occurred during nighttime hours when high resolution
visible imagery was not available.

33

Figure 25a.--Enlarged area from 2-km equivalent IR produced using digital enhancement (Mb curve), 2000 GMT, 13 June 1976.

Figure 25b.--Enlarged area from 2-km visible imagery, 2000 GMT, 13 June 1976.
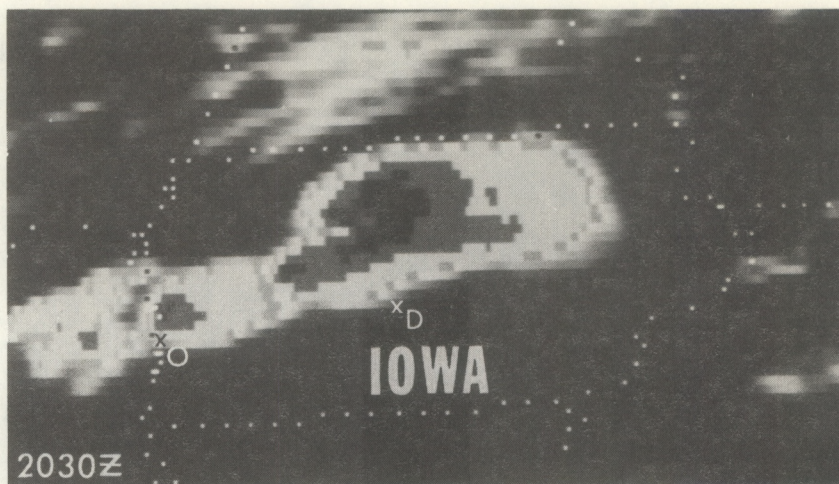
Figure 26a.--Enlarged area from 2-km equivalent IR produced using digital enhancement (Mb curve), 2030 GMT, 13 June 1976.
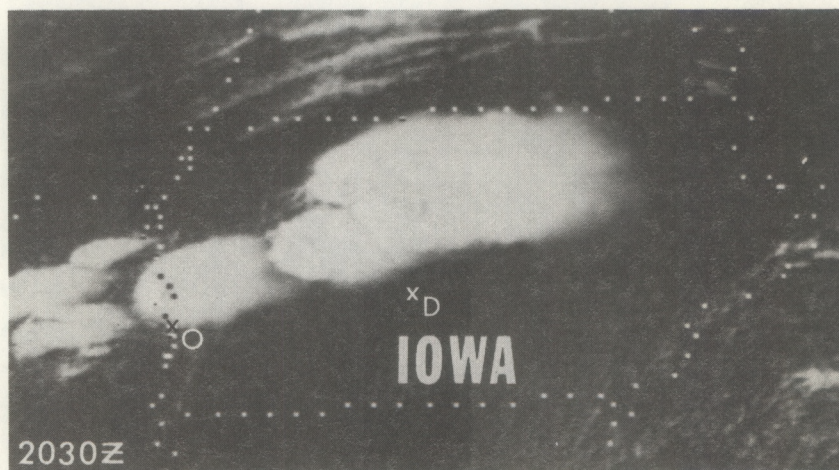
Figure 26b.--Enlarged area from 2-km visible imagery, 2030 GMT, 13 June 1976.
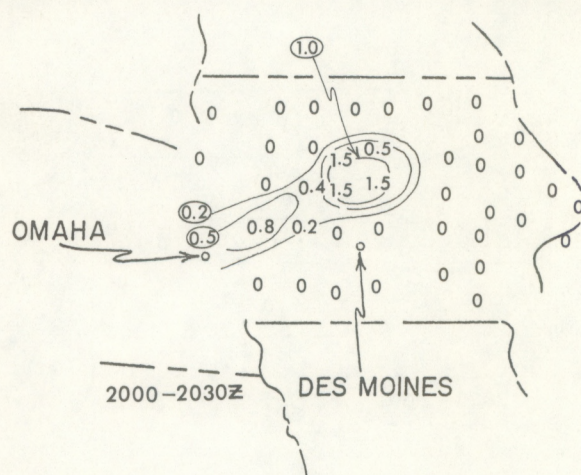
Figure 26c.--Half-hour rainfall estimate in inches using the decision tree, 2000-2030 GMT, 13 June 1976; analyzed rainfall values are circled.
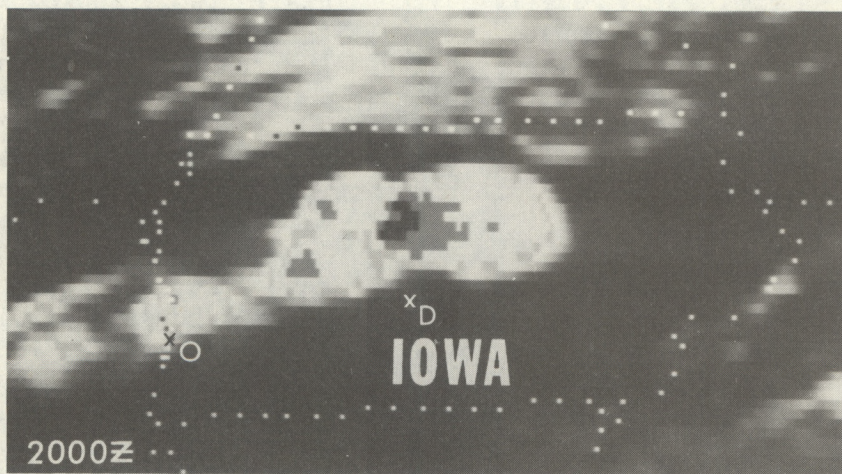
35
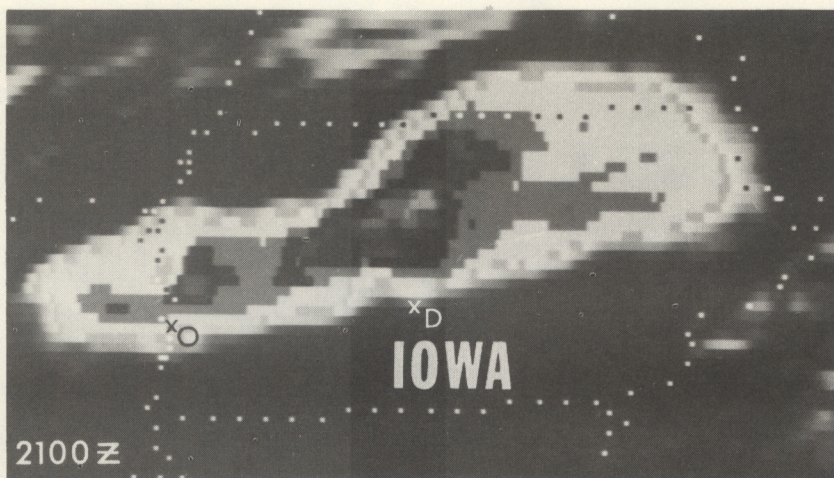
Figure 27a.--Enlarged area from 2-km equivalent IR produced using digital
enhancement (Mb curve), 2100 GMT, 13 June 1976.

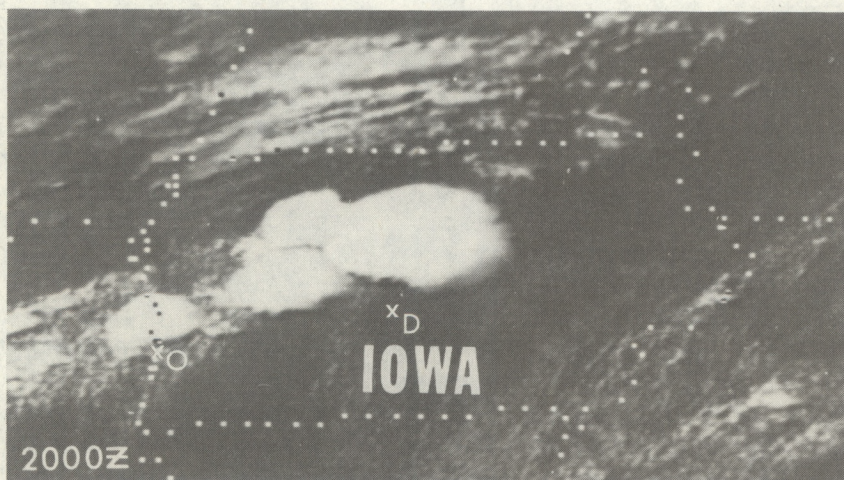Figure 27b.--Enlarged area from 2-km visible imagery, 2100 GMT, 13 June 1976.
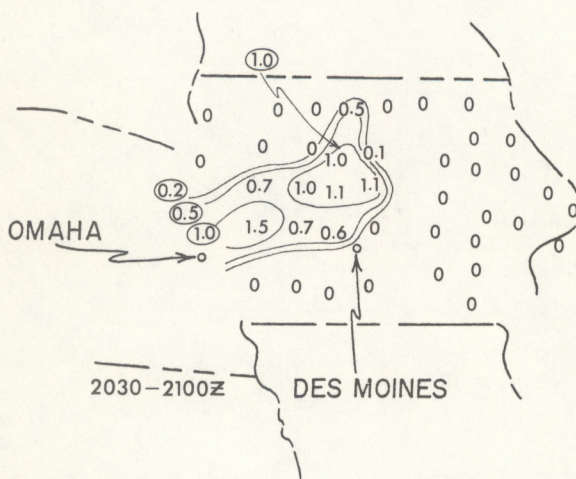
Figure 27c.--Half-hour rainfall estimate in inches using the decision tree,
2030-2100 GMT, 13 June 1976; analyzed rainfall values are
circled.

36
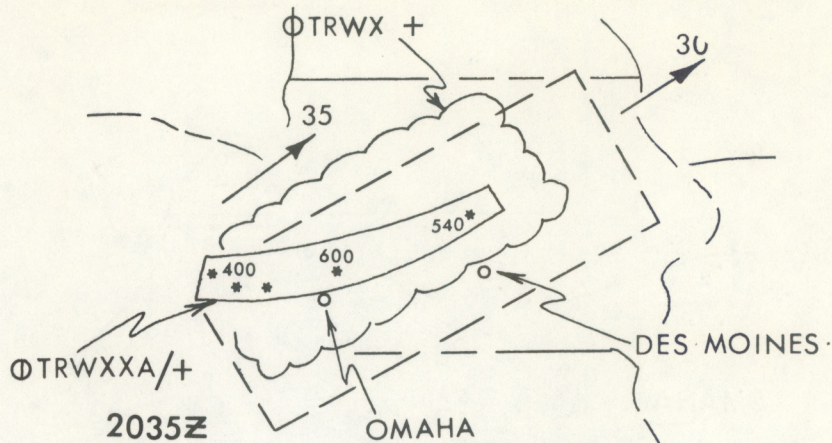
Figure 28a.--Radar analysis, 2035 GMT, 13 June 1976.
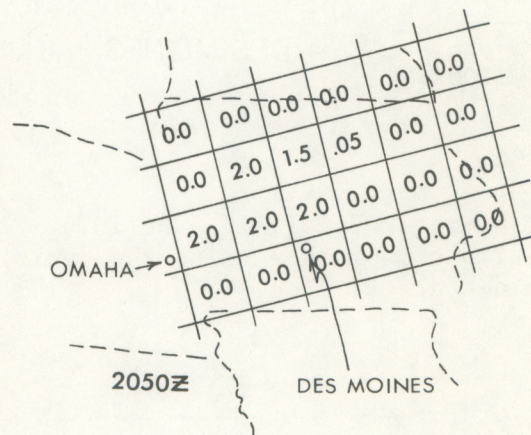
Figure 28b.--Rainfall values in inches obtained from Manually Digitized
Radar (MDR) Data, 2050 GMT, 13 June 1976.
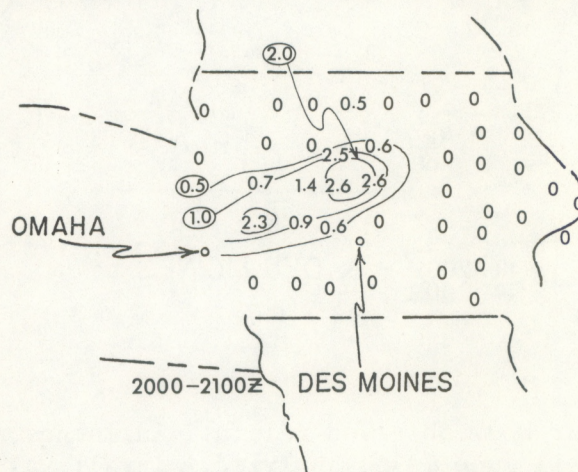
Figure 28c.--One Hour, 2000-2100 GMT, 13 June 1976, satellite-derived rainfall
estimate in inches, obtained by summing the two half-hourly
intervals, 2000-2030 GMT and 2030-2100 GMT; analyzed rainfall
values are circled.

37
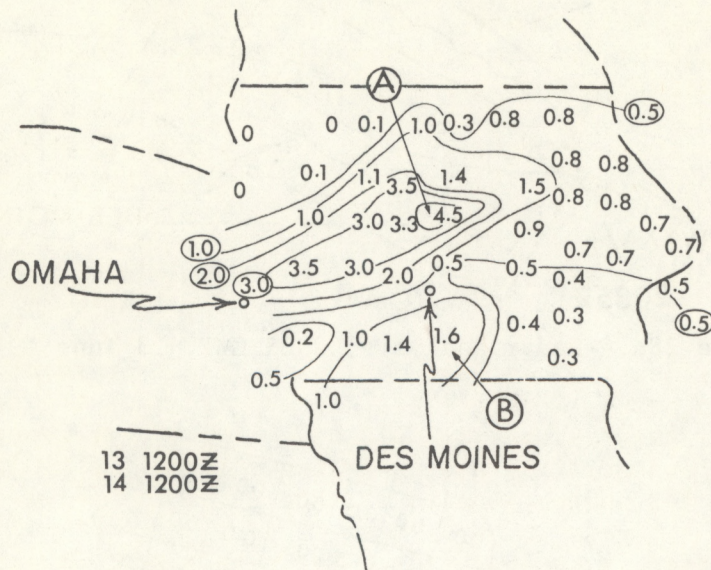
Figure 29a.--Twenty-four hour, 1200 GMT, 13 June 1976 - 1200 GMT, 14 June 1976, rainfall estimate in inches using the decision tree; analyzed rainfall values are circled.
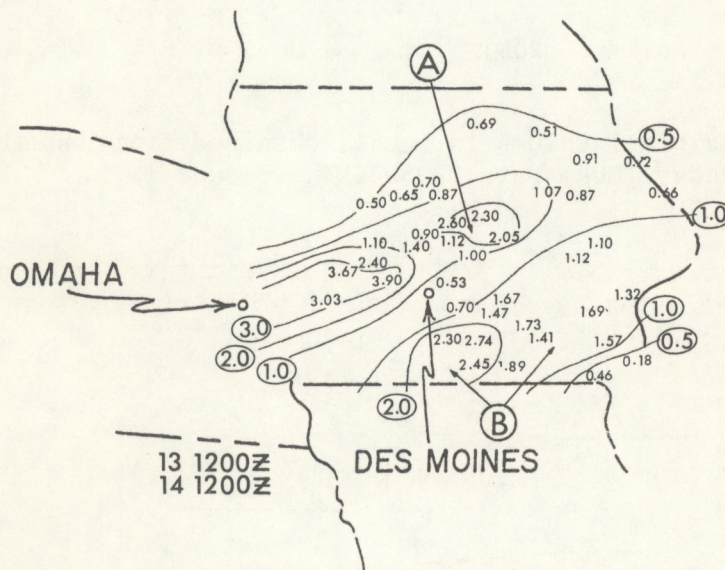
Figure 29b.--Twenty-four hour observed rainfall in inches, 1200 GMT, 13 June - 1200 GMT, 14 June 1976; analyzed rainfall values are circled.

IV. ADDITIONAL COMMENTS ON THE RAINFALL ESTIMATION SCHEME

Some limited testing of this scheme has also been done with hurricanes. The results seem encouraging, particularly for pinpointing locally heavy rain areas in real-time for both thunderstorm systems and hurricanes. Depending on the size and intensity of the systems under investigation, rainfall estimates should be made at a sufficient number of convective points in order to obtain a detailed analysis of the rainfall.

Even though this scheme estimates rainfall at a point, the contours in the enhanced IR imagery associated with the active portion of the Cb system actually represent estimated isohyets of rainfall as a "first guess" from Step 4 in the Decision Tree. This "first guess" isohyet analysis is then refined if precipitation amplifiers (in Step 5 of the Decision Tree) are present.

Only limited verification has been done partially because of the sparsity of rainfall observations. Nevertheless, it appears that the scheme, on the average, underestimates the rainfall up to 30% in extreme rainfall situations (≥ 2 inches/hour) and overestimates rainfall up to 30% for light to heavy rainfalls (<2 inches/hour).

An important problem is separating the inactive cirrus debris from the active cloud elements producing significant rainfall. This problem is most noticeable when estimating rainfall from hurricanes, particularly when they interact with the westerlies and associated baroclinic zones. The problem is partially solved by using IR to locate the coldest tops and the tighter IR temperature gradients which usually pinpoint the area of significant rainfall. Also, bright-textured clouds and overshooting tops in the high resolution visible imagery usually locate the important rainfall areas.

Another way of separating out the cirrus debris is by animation. Anvil cirrus normally move in the direction of the wind at cirrus level. The significant rainfall associated with the Cb cells often moves in a different direction from the cirrus debris.

Another important variable is the variation in the tropopause height. We designed the system using summer tropopauses with temperatures between -60 to -66°C. However, tropopauses do occur at lower heights (warmer temperatures). For such cases, several of the colder gray shades may not show up even though the convection is vigorous enough to penetrate the lower tropopause. Either the Decision Tree or the gray shade enhancement program could be revised so that the tropopause temperature is considered more adequately.

V.   CONCLUSIONS

Hydrologists and river forecasters occasionally need to make quick decisions in a precipitation situation. Satellite imagery has the potential of aiding the hydrologist in his evaluation or prediction of the flood potential. There are certain patterns and ongoing changes in the enhanced IR and visible imagery that appear to be associated with locally heavy rains:

(1) Quasi-stationary Cb systems; Cb systems regenerating from same location.

(2) Cold, <u>rapidly</u> expanding Cb anvils.

(3) Cb mergers.

(4) Merging convective cloud lines.

(5) Overshooting tops.

Also, the Decision Tree method outlined in this paper can be used for making rainfall evaluations quickly. This method represents only the initial phase of the development needed for a scheme that can be used universally for estimating rain from convective storms. The scheme and the estimates from it should be fine-tuned for local terrain differences and for climate. For example, in mountainous terrain in the drier parts of the United States, we know that most thunderstorms drop much more rain on the upper parts of the mountain than in the valleys. Much of the rain evaporates before it reaches the lower levels. Fine-tuning of the estimations in such an area would take into account the normal distribution of rainfall with height (for convective rains) if known, or just the height if the climatology is not known. In very moist mountainous climates the rainfall rates would be just as great or greater at the lower levels than higher up, however, the frequency would be much greater on the slopes, and mergers would be almost continuous when the wind was advecting clouds into a converging valley.

Each area forecaster should determine for himself, the range of each rainfall value as a function of cloud temperature and rate of cloud temperature changes, using the value of each estimate in the Decision Tree as guidance. Also, each forecast office should test various curves to determine the best IR enhancement for estimating convective rainfall.

In areas where satellite pictures, high quality radar data, and a high density of surface rain gauge data are available, these data should be used in combination for the most accurate precipitation results. At present, the new manually digitized radar of approximately 22x22 nm resolution and the National Weather Service remote PPI display combined with the satellite pictures offer the greatest possibility for improved rainfall estimates considering the time and effort spent; it is with this combination that we plan to continue this work over the U.S.

ACKNOWLEDGMENTS

REFERENCES

Follansbee, Walton A. and Oliver, V. J., 1975: A Comparison of Infrared Imagery and Video Pictures in the Estimation of Daily Rainfall from Satellite Data. NOAA Technical Memorandum NESS 62, 14 pp.

Follansbee, Walton A., 1976: Estimation of Daily Precipitation over China and the U.S.S.R. using Satellite Imagery. NOAA Technical Memorandum NESS 81, 30 pp.

Fujita, Theodore T., 1972: Tornado Occurrences Related to Overshooting Cloud-top Heights as Determined from ATS Pictures, SMRP Research Paper 97, 32 pp.

Griffith, Cecilia G., Woodley, W. L. and Martin, D. W., et al., 1976: Rainfall Estimation from Geosynchronous Satellite Imagery during Daylight Hours. NOAA Technical Report ERL 356-WMPO7, 106 pp.

Martin, David W. and Scherer, W. D., 1973: Review of Satellite Rainfall Estimation Methods. Bulletin American Meteorological Society, 56, pp. 9-12.

Martin, David W., Stout, J. and Sikdar, D. N., 1975: GATE Area Rainfall Estimation from Satellite Images. A report on NOAA Grant 04-5-158-47, 28 pp.

Oliver, Vincent J. and Scofield, R. A., 1976: Estimation of Rainfall from Satellite Imagery. Published in the preprint volumes from both the Conference on Hydro-Meteorology, April 20-22, 1976, Ft. Worth, Texas, and the Sixth Conference on Weather Forecasting and Analysis, May 10-14, 1976.

Shenk, William E., 1974: Cloud Top Height Variability of Strong Convective Cells. Journal Applied Meteorology, 13, pp. 917-922.

Simpson, Joanne and Woodley, W. L., 1971: Seeding Cumulus in Florida: New 1970 Results. Science, 172, pp. 117-126.

Woodley, William L., Sancho, B. and Miller, A. H., 1972: Rainfall Estimation from Satellite Cloud Photographs. NOAA Technical Memorandum ERL OD-11, 43 pp.

Woodley, William L. and Sax, R. I., 1976: The Florida Area Cumulus Experiment: Rationale, Design, Procedures, Results and Future Course. NOAA Technical Report ERL 354-WMPO6, 204 pp.

APPENDIX

Half-hourly convective rainfall estimation scheme (in inches) at a station; enhanced IR and high resolution visible imagery used as input.

DECISION TREE

START

IR & VIS

Is the cloud convective?

No ⟶ Stop

Yes

IR

Does cloud top reach first level of contoured enhancement?

No ⟶ 0.05 inches; enter .05 in Step 6 Total

Yes ⟶ Go to Step 3
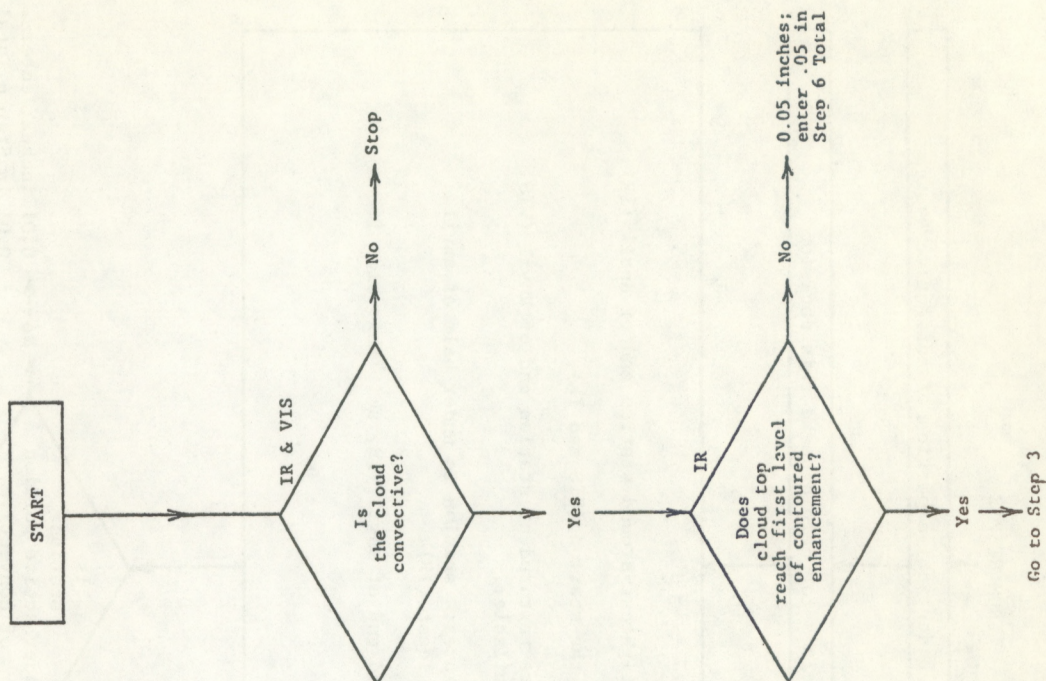
STEP 1.
Examine shape of cloud to determine if convective (round, oval, carrot-shaped, triangular). USE VIS AND IR.

STEP 2.
Determine if convection is deep. USE ENHANCED IR.

43

FROM STEP 2

Determine if station is under active portion of convective system

The following are clues for helping make this decision

1. IR temperature gradient is tightest around station end of anvil (IR).

2. An overshooting top is over the station (VIS and IR).

3. Anvil is brighter and/or more textured at station end of anvil (VIS, skip this clue if no VIS available).

4. From comparing last two pictures: station is under half of anvil bounded by edge which moves least (IR).

5. Station is near 300 mb upwind end of anvil (IR, skip this clue if no upper air data available).

Is station under active portion of convective system?

No → 0.01 inches; enter 0.01 in Step 6 Total

Yes

GO TO STEP 4

STEP 3.
Identify the active portion of the convective cloud system. Use enhanced IR and VIS. VIS (underlined) means that visible imagery is the best data for making that decision.

A. Upwind portion of anvil locates the active area of the convective system:

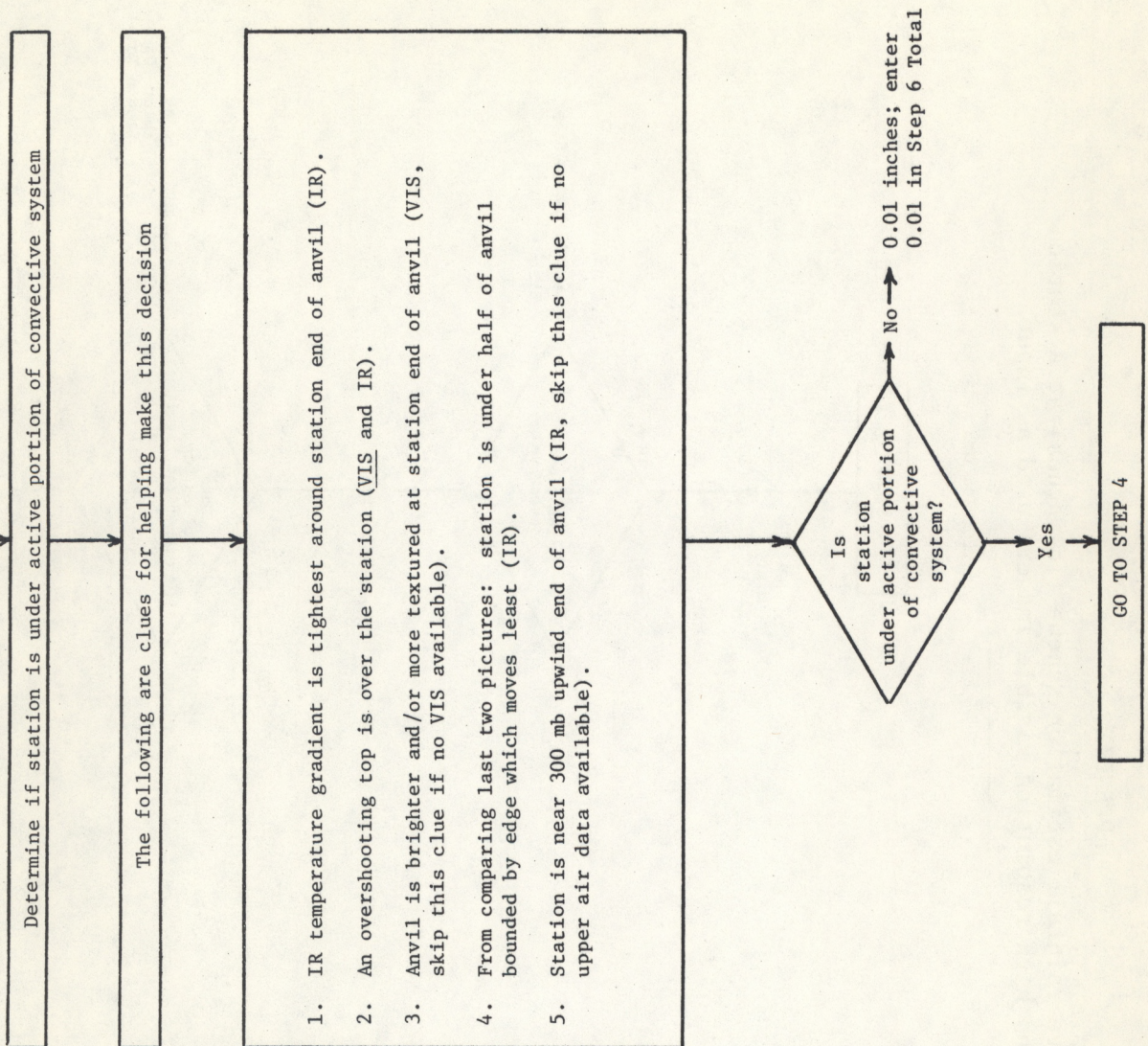IR gradient is tightest around upwind end of anvil.

Clouds are brightest and sometimes textured at upwind end.

Comparison of two successive pictures shows motion of anvil edge; greatest in downwind direction.

Winds aloft (usually best at 300 mb) used for determining upwind direction.

B. Overshooting tops show active area of anvil.

44

STEP 4.
Estimate half-hourly precip rates as a function of cloud top temperature and temperature change. USE ENHANCED IR.

• Rainfall is heaviest when and where clouds are still getting colder and coldest area is growing.

From Step 3 → IR → **Did the coldest clouds in the anvil increase in area?**

No → IR → **Did the coldest cloud remain the same?**

No → IR → **Did the coldest clouds contract, become warmer or detach from its roots?**

Yes (from "increase in area?") → **Determine amount that the coldest cloud tops increased within half-hour**

CLOUD TEMPERATURE	Determine amount that the coldest cloud tops increased within half-hour				
	>2/3°Lat	>1/3≤2/3	≤1/3	Yes	T
Medium Gray (-32 to -41°C)	0.25	0.15	0.10	0.05	T
Light Gray (-41 to -52°C)	0.50	0.20	0.15	0.10	0.01
Dark Gray (-52 to -58°C)	0.75	0.40	0.20	0.15	0.03
Black (-58 to -62°C)	1.00	0.60	0.30	0.20	0.05
Repeat Gray Levels (-62 to -80°C)	1.50	0.75	0.40	0.30	0.08
White (Below -80°C)	2.00	1.00	0.50	0.40	0.10

First Guess Estimate → Enter First Guess in Step 6 and go to Step 5

STEP 5.
Analyze imagery for presence of precip amplifiers.
USE VIS AND ENHANCED IR. VIS (underlined) means that visible imagery is the best data for making that decision.
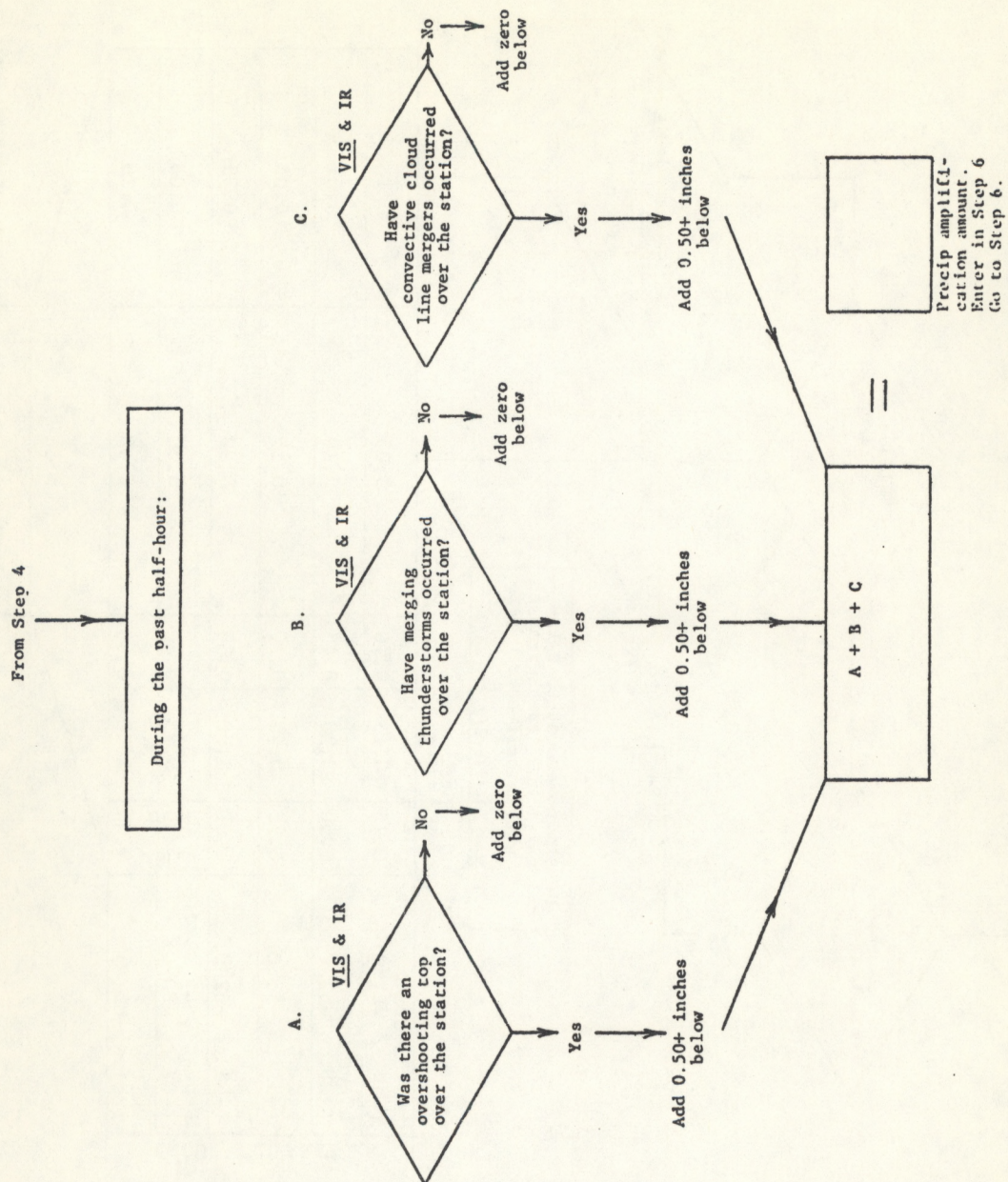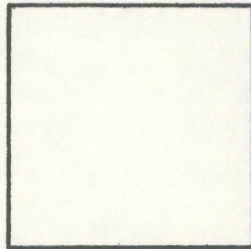
Overshooting tops.

Cell mergers.

Line mergers.

From Step 4

During the past half-hour:

A. VIS & IR
Was there an overshooting top over the station?
No → Add zero below
Yes → Add 0.50+ inches below

B. VIS & IR
Have merging thunderstorms occurred over the station?
No → Add zero below
Yes → Add 0.50+ inches below

C. VIS & IR
Have convective cloud line mergers occurred over the station?
No → Add zero below
Yes → Add 0.50+ inches below

A + B + C

=

Precip amplification amount. Enter in Step 6. Go to Step 6.

46

STEP 6.
Total Estimate.

$$\boxed{} \;+\; \boxed{} \;=\; \boxed{}$$

First guess from Step 4.

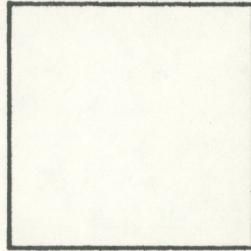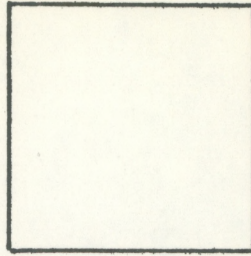Precipitation amplification amount from Step 5.

Total Estimate (Steps 2, 3)

NOAA TECHNICAL MEMORANDUMS

National Environmental Satellite Service Series

The National Environmental Satellite Service (NESS) is responsible for the establishment and operation of the environmental satellite systems of NOAA.

NOAA Technical Memorandums facilitate rapid distribution of material that may be preliminary in nature and so may be published formally elsewhere at a later date. Publications 1 through 20 and 22 through 25 are in the earlier ESSA National Environmental Satellite Center Technical Memorandum (NESCTM) series. The current NOAA Technical Memorandum NESS series includes 21, 26, and subsequent issuances.

Publications listed below are available from the National Technical Information Service, U.S. Department of Commerce, Sills Bldg., 5285 Port Royal Road, Springfield, Va. 22151. Prices on request. Order by accession number (given in parentheses). Information on memorandums not listed below can be obtained from Environmental Data Service (D831), 3300 Whitehaven St., NW., Washington, D.C. 20235.

NESS 45   A Technique for the Analysis and Forecasting of Tropical Cyclone Intensities From Satellite Pictures (Revision of NESS 36). Vernon F. Dvorak, February 1973, 19 pp. (COM-73-10675)

NESS 46   Publications and Final Reports on Contracts and Grants, 1972. NESS, April 1973, 10 pp. (COM-73-11035)

NESS 47   Stratospheric Photochemistry of Ozone and SST Pollution: An Introduction and Survey of Selected Developments Since 1965. Martin S. Longmire, March 1973, 29 pp. (COM-73-10786)

NESS 48   Review of Satellite Measurements of Albedo and Outgoing Long-Wave Radiation. Arnold Gruber, July 1973, 12 pp. (COM-73-11443)

NESS 49   Operational Processing of Solar Proton Monitor Data. Louis Rubin, Henry L. Phillips, and Stanley R. Brown, August 1973, 17 pp. (COM-73-11647/AS)

NESS 50   An Examination of Tropical Cloud Clusters Using Simultaneously Observed Brightness and High Resolution Infrared Data From Satellites. Arnold Gruber, September 1973, 22 pp. (COM-73-11941/4AS)

NESS 51   SKYLAB Earth Resources Experiment Package Experiments in Oceanography and Marine Science. A. L. Grabham and John W. Sherman, III, September 1973, 72 pp. (COM 74-11740/AS)

NESS 52   Operational Products From ITOS Scanning Radiometer Data. Edward F. Conlan, October 1973, 57 pp. (COM-74-10040)

NESS 53   Catalog of Operational Satellite Products. Eugene R. Hoppe and Abraham L. Ruiz (Editors), March 1974, 91 pp. (COM-74-11339/AS)

NESS 54   A Method of Converting the SMS/GOES WEFAX Frequency (1691 MHz) to the Existing APT/WEFAX Frequency (137 MHz). John J. Nagle, April 1974, 18 pp. (COM-74-11294/AS)

NESS 55   Publications and Final Reports on Contracts and Grants, 1973. NESS, April 1974, 8 pp. (COM-74-11108/AS)

NESS 56   What Are You Looking at When You Say This Area Is a Suspect Area for Severe Weather? Arthur H. Smith, Jr., February 1974, 15 pp. (COM-74-11333/AS)

NESS 57   Nimbus-5 Sounder Data Processing System, Part I: Measurement Characteristics and Data Reduction Procedures. W.L. Smith, H. M. Woolf, P. G. Abel, C. M. Hayden, M. Chalfant, and N. Grody, June 1974, 99 pp. (COM-74-11436/AS)

NESS 58   The Role of Satellites in Snow and Ice Measurements. Donald R. Wiesnet, August 1974, 12 pp. (COM-74-11747/AS)

NESS 59   Use of Geostationary-Satellite Cloud Vectors to Estimate Tropical Cyclone Intensity. Carl. O. Erickson, September 1974, 37 pp. (COM-74-11762/AS)

NESS 60   The Operation of the NOAA Polar Satellite System. Joseph J. Fortuna and Larry N. Hambrick, November 1974, 127 pp. (COM-75-10390/AS)

NESS 61   Potential Value of Earth Satellite Measurements to Oceanographic Research in the Southern Ocean. E. Paul McClain, January 1975, 18 pp. (COM-75-10479/AS)

NESS 62   A Comparison of Infrared Imagery and Video Pictures in the Estimation of Daily Rainfall From Satellite Data. Walton A. Follansbee and Vincent J. Oliver, January 1975, 14 pp. (COM-75-10435/AS)

NOAA SCIENTIFIC AND TECHNICAL PUBLICATIONS

NOAA, the *National Oceanic and Atmospheric Administration,* was established as part of the Department of Commerce on October 3, 1970. The mission responsibilities of NOAA are to monitor and predict the state of the solid Earth, the oceans and their living resources, the atmosphere, and the space environment of the Earth, and to assess the socioeconomic impact of natural and technological changes in the environment.

The six Major Line Components of NOAA regularly produce various types of scientific and technical information in the following kinds of publications:

PROFESSIONAL PAPERS — Important definitive research results, major techniques, and special investigations.

TECHNICAL REPORTS—Journal quality with extensive details, mathematical developments, or data listings.

TECHNICAL MEMORANDUMS — Reports of preliminary, partial, or negative research or technology results, interim instructions, and the like.

CONTRACT AND GRANT REPORTS—Reports prepared by contractors or grantees under NOAA sponsorship.

TECHNICAL SERVICE PUBLICATIONS—These are publications containing data, observations, instructions, etc. A partial listing: Data serials; Prediction and outlook periodicals; Technical manuals, training papers, planning reports, and information serials; and Miscellaneous technical publications.

ATLAS—Analysed data generally presented in the form of maps showing distribution of rainfall, chemical and physical conditions of oceans and atmosphere, distribution of fishes and marine mammals, ionospheric conditions, etc.
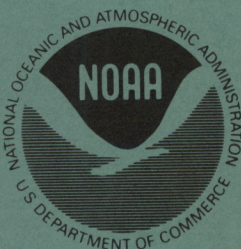
Information on availability of NOAA publications can be obtained from:

**ENVIRONMENTAL SCIENCE INFORMATION CENTER
ENVIRONMENTAL DATA SERVICE
NATIONAL OCEANIC AND ATMOSPHERIC ADMINISTRATION
U.S. DEPARTMENT OF COMMERCE**

**3300 Whitehaven Street, N.W.
Washington, D.C. 20235**

NOAA--S/T 77-2658